Topographic brain tumor anatomy drives seizure risk and enables machine learning based prediction

Akeret, Kevin ; Stumpo, Vittorio ; Staartjes, Victor E ; Vasella, Flavio ; Velz, Julia ; Marinoni, Federica ; Dufour, Jean-Philippe ; Imbach, Lukas L ; Regli, Luca ; Serra, Carlo ; Krayenbühl, Niklaus

Abstract: OBJECTIVE The aim of this study was to identify relevant risk factors for epileptic seizures upon initial diagnosis of a brain tumor and to develop and validate a machine learning based prediction to allow for a tailored risk-based antiepileptic therapy. METHODS Clinical, electrophysiological and high-resolution imaging data was obtained from a consecutive cohort of 1051 patients with newly diagnosed brain tumors. Factor-associated seizure risk difference allowed to determine the relevance of specific topographic, demographic and histopathologic variables available at the time of diagnosis for seizure risk. The data was divided in a 70/30 ratio into a training and test set. Different machine learning based predictive models were evaluated before a generalized additive model (GAM) was selected considering its traceability while maintaining high performance. Based on a clinical stratification of the risk factors, three different GAM were trained and internally validated. RESULTS A total of 923 patients had full data and were included. Specific topographic anatomical patterns that drive seizure risk could be identified. The involvement of allopallial, mesopallial or primary motor/somatosensory neopallial structures by brain tumors results in a significant and clinically relevant increase in seizure risk. While topographic input was most relevant for the GAM, the best prediction was achieved by a combination of topographic, demographic and histopathologic information (Validation: AUC: 0.79, Accuracy: 0.72, Sensitivity: 0.81, Specificity: 0.66). CONCLUSIONS This study identifies specific phylogenetic anatomical patterns as epileptic drivers. A GAM allowed the prediction of seizure risk using topographic, demographic and histopathologic data achieving fair performance while maintaining transparency.

DOI: https://doi.org/10.1016/j.nicl.2020.102506

Topographic brain tumor anatomy drives seizure risk and enables machine learning based prediction. NeuroImage: Clinical, 28:102506.
DOI: https://doi.org/10.1016/j.nicl.2020.102506

NeuroImage: Clinical 28 (2020) 102506

Contents lists available at ScienceDirect

NeuroImage: Clinical

journal homepage: www.elsevier.com/locate/ynicl

Topographic brain tumor anatomy drives seizure risk and enables machine learning based prediction

Kevin Akeret [a,*,1], Vittorio Stumpo [a,b,1], Victor E. Staartjes [a,c], Flavio Vasella [a], Julia Velz [a], Federica Marinoni [a], Jean-Philippe Dufour [a], Lukas L. Imbach [d], Luca Regli [a], Carlo Serra [a,1], Niklaus Krayenbühl [a,e,1]

[a] Department of Neurosurgery, Clinical Neuroscience Center, University Hospital Zurich, University of Zurich, Zurich, Switzerland
[b] Institute of Neurosurgery, Università Cattolica del Sacro Cuore, Rome, Italy
[c] Amsterdam UMC, Vrije Universiteit Amsterdam, Neurosurgery, Amsterdam Movement Sciences, Amsterdam, The Netherlands
[d] Division of Epileptology, Department of Neurology, Clinical Neuroscience Center, University Hospital Zurich, University of Zurich, Zurich, Switzerland
[e] Division of Pediatric Neurosurgery, University Children's Hospital, Zurich, Switzerland

ARTICLE INFO

Keywords:
Epilepsy
Metastases
Glioma
Primary central nervous system lymphoma
Generalized additive model

ABSTRACT

Objective: The aim of this study was to identify relevant risk factors for epileptic seizures upon initial diagnosis of a brain tumor and to develop and validate a machine learning based prediction to allow for a tailored risk-based antiepileptic therapy.

Methods: Clinical, electrophysiological and high-resolution imaging data was obtained from a consecutive cohort of 1051 patients with newly diagnosed brain tumors. Factor-associated seizure risk difference allowed to determine the relevance of specific topographic, demographic and histopathologic variables available at the time of diagnosis for seizure risk. The data was divided in a 70/30 ratio into a training and test set. Different machine learning based predictive models were evaluated before a generalized additive model (GAM) was selected considering its traceability while maintaining high performance. Based on a clinical stratification of the risk factors, three different GAM were trained and internally validated.

Results: A total of 923 patients had full data and were included. Specific topographic anatomical patterns that drive seizure risk could be identified. The involvement of allopallial, mesopallial or primary motor/somatosensory neopallial structures by brain tumors results in a significant and clinically relevant increase in seizure risk. While topographic input was most relevant for the GAM, the best prediction was achieved by a combination of topographic, demographic and histopathologic information (*Validation:* AUC: 0.79, Accuracy: 0.72, Sensitivity: 0.81, Specificity: 0.66).

Conclusions: This study identifies specific phylogenetic anatomical patterns as epileptic drivers. A GAM allowed the prediction of seizure risk using topographic, demographic and histopathologic data achieving fair performance while maintaining transparency.

1. Introduction

Seizures represent a burdensome comorbidity to patients with brain tumors, occurring in 30–50% of patients, yet the role of prophylactic treatment remains controversial (Fisher et al., 2017, 2014; van Breemen et al., 2007). Although prophylactic anticonvulsant therapy for newly diagnosed brain tumors is not recommended (Glantz et al., 2000; Sirven et al., 2004; Tremont-Lukats et al., 2008), this issue remains controversial and the practice varies widely across different centers and countries (Siomin et al., 2005). Seizure risk stratification at diagnosis of the brain tumor would substantially contribute to this dispute and in addition inform the nature of surveillance and the potential benefit of lifestyle changes (Rossetti and Stupp, 2010). However, insufficient pathophysiological insight into the role of risk factors has rendered accurate prediction difficult.

Anatomical features of primary brain tumors have been shown to

* Corresponding author.
E-mail addresses: kevin.akeret@usz.ch, kevin.akeret@gmx.ch (K. Akeret).
[1] These authors contributed equally to the manuscript. K. Akeret and V. Stumpo share first authorship. C. Serra and N. Krayenbühl share senior authorship.

https://doi.org/10.1016/j.nicl.2020.102506
Received 11 August 2020; Received in revised form 5 October 2020; Accepted 10 November 2020
Available online 19 November 2020

impact seizure risk and semiology (Akeret et al., 2019). One advantage of anatomical information derives from its availability at time of diagnosis thanks to modern neuroimaging. Histopathologic tumor entity and molecular markers have also been associated with seizure risk (Ertürk Çetin et al., 2017; Kerkhof and Vecht, 2013; Pallud et al., 2014; Sanson et al., 2009; Skardelly et al., 2015), but these have the disadvantage of being available late in the diagnostic process. While experienced clinicians may be able to estimate the most probable entity of the underlying tumor, the definitive diagnosis only becomes available late in the diagnostic process. Machine learning (ML) provides new approaches for prediction, often outperforming conventional statistical methods (Rajkomar et al., 2019; Staartjes et al., 2018; Swinburne et al., 2019; Titano et al., 2018; van Niftrik et al., 2019). However, transparency and pathophysiological plausibility remain important concerns, contributing to the limited translation into clinical practice (Rajkomar et al., 2019). ML methods differ in terms of their transparency. Generalized additive models (GAM) offer the specific advantage that they can arrive at predictions with high accuracy while still remaining explainable, as smooth partial dependences can be derived to illustrate the influence of every feature (Hastie and Tibshirani, 1986). ML based methods have been applied in various areas of epilepsy research (Abbasi and Goldenholz, 2019; Arle et al., 1999; Gleichgerrcht et al., 2018; Munsell et al., 2015), yet never to predict the risk of seizures using anatomical data.

This study aims at a comprehensive assessment of the risk factors for epileptic seizures in parenchymal brain tumors and their predictive potential using a ML based approach. An improved pathophysiological understanding of the drivers for epileptic seizures and their implementation in a prediction model has the potential to provide a tailored antiepileptic treatment approach in patients with newly diagnosed brain tumors.

2. Materials and methods

This study is reported in accordance with the STROBE (von Elm et al., 2007) and TRIPOD (Moons et al., 2015) statements.

2.1. Source population

The data was obtained consecutively over an eight-year period (January 2009 to December 2016) from patients with a newly diagnosed brain tumor admitted to our tertiary care hospital. The eligibility criteria comprised: (i) Primary diagnosis with consecutive histopathologic confirmation of a primary or secondary brain tumor, (ii) no pretreatment or previous cranial surgery, (iii) intraparenchymal encephalic tumor location (supra-, infratentorial or both), exclusion of extraaxial or spinal tumors, (iv) availability of complete preoperative high resolution magnetic resonance imaging (MRI) data (technical details in *supplementary methods*), (v) determinable seizure status preoperatively, (vi) no prophylactic antiepileptic treatment and (vii) quantifiable number of lesions (see below).

2.2. Data collection

The study was approved by the local ethics committee (KEK 01120). Supplementary Table 1 provides the demographic, clinical and histopathologic data obtained with the respective specifications. Clinical and electrophysiological investigations regarding epileptic seizures were performed preoperatively in a specialized epilepsy unit. Seizure prevalence was assessed based on patient history and description by family members for epileptic events. In cases of diagnostic uncertainty, laboratory values were consulted and inter-ictal electroencephalography (EEG) or long-term EEG performed to inform clinical decision making. The assessment of seizure semiology followed the 2017 International League Against Epilepsy Classification (Fisher et al., 2017). Histopathologic analysis was performed by our hospital's Institute of Neuropathology.

2.3. Brain segmentation and tumor anatomy classification

The classification of anatomical brain tumor features followed a predefined segmentation scheme (Akeret et al., 2020), described in Supplementary Table 2 and illustrated in Supplementary Fig. 1. The segmentation is based on the Terminologia Anatomica (Allen, 2009). The assessment of the anatomical brain tumor features was performed on preoperative high-resolution MRI. Image analysis was independently conducted by two assessors (KA and CS) masked to demographic and histopathologic patient characteristics. In cases of disagreement a consensus was obtained by consulting the senior author (NK). The topographic anatomical parameters were analyzed separately for each patient and coded binarily (tumor affected vs. non-affected, applicable vs. non-applicable) by combining the morphological sequences (T1, T1 with contrast, T2 and FLAIR). Structures considered as displaced or with edematous changes only were classified as non-infiltrated. Patients with more than ten encephalic lesions were excluded.

2.4. Statistical analysis

Continuous data are given as mean and standard deviation, categorical data as absolute numbers and percentages. Seizure risk and semiology are provided with a 95% confidence interval (Wilson). Seizure risk difference represents the absolute risk difference between binary variables (eg. seizure risk if anatomical structures affected minus seizure risk if anatomical structure not affected) or to the indicated reference within categorical variables with more than two levels (eg. histological entity with glioblastoma as reference). Seizure risk difference is given with a 95% confidence interval (Wilson). For certain histopathologic entities, grouping was performed to increase statistical power (eg. combination of dysembryoplastic neuroepithelial tumors (DNET) and ganglioglioma to developmental tumors).

2.5. Predictive modeling strategy

Missing data imputation was not required as only patients with complete data were included in the study. Topographic features were one-hot encoded for the machine learning models. Seizure occurrence was used as binary endpoint. The dataset was randomly split into training and testing set in a 70/30 ratio (n = 646/277). To counteract class imbalance, conventional random upsampling was applied (Staartjes and Schröder, 2018). Input variable selection was performed on the training dataset using random forest-based recursive feature elimination (RFE) with bootstrap resampling (Guyon et al., 2002). Model selection was based on resampled out-of-the-box performance on the training set. We initially evaluated the following models: *generalized linear model* (glm), *random forest* (rf), *C5.0 decision tree*, *gradient boosting machine* (gbm), *neural network* (nnet), *radial kernel support vector machine* (svmRadial) and GAM. Bootstrapping with replacement in 25 repetitions was used to train the different models and to assess out-of-sample error. As it provided similar performance, but higher interpretability, the GAM was chosen.

In a second step, after ideal model selection, RFE was performed on 3 different set of strictly non-redundant variables: 1. *Topographic* (T) – including only anatomical data; 2. *Topographic/Demographic* (TD) – also including age and gender; and 3. *Topographic/Demographic/Histopathologic* (TDH) – with the additional inclusion of histological entity and WHO grade. GAM were trained on the training patient set for each of the 3 different variables combinations obtained after RFE. For each, area under the curve (AUC), accuracy, sensitivity, specificity, calibration slope and intercept with the corresponding 95% confidence intervals were calculated and taken into consideration.

The *T, TD* and *TDH* GAM were internally validated on the testing set. Explanation of model-internal variable weighting was possible through calculation of partial dependenc (PD) values. For each variable in a GAM, PD describes the marginal effect that a specific input has on the

outcome. The advantage is that - in contrast to generic measures of variable importance available for other ML models - this is not a mere ranking according to importance, but additionally the directions, extent, and distribution of the marginal effects can be illustrated. As the TDH model was found to have best performance, PD was calculated for its variables. R 3.5.3. was used for all analyses (R Core Team, 2020).

2.6. Data availability

The authors confirm that the data supporting the findings of this study are available within the article and its Supplementary materials. Raw data are available from the corresponding author (KA) upon reasonable request.

3. Results

3.1. Study population

Details on the cohort's eligibility assessment are provided in Supplementary Fig. 2. Of 1051 screened patients, 923 could be included in the study. The mean age of the study population was 53.6 years (SD 19.6). Details on demographic and histopathologic characteristics are shown in Table 1.

4. Seizure prevalence

Topographic tumor anatomy is given in Table 2 *and* Supplementary Table 3. The overall prevalence of epileptic seizures was 37.6%. Seizure semiology is shown in Supplementary Table 4. Focal to bilateral tonic-clonic seizures were most prevalent (50%), followed by focal motor seizures with intact awareness (18%).

Seizure prevalence and seizure risk difference in relation to demographic and histopathologic characteristics are given in Fig. 1 and Table 1. Seizure risk peaks between age 30 to 50 years. No gender difference was observed. Compared to patients with glioblastoma, patients with an astrocytoma (diffuse or anaplastic), an oligoastrocytoma (diffuse or anaplastic) or a developmental tumor (DNET or ganglioglioma) showed an increased risk of seizures. Pilocytic astrocytoma, medulloblastoma, ependymoma and the group summarized here as miscellaneous neuroepithelial tumors had a reduced risk of epileptic seizures. PCNSL and metastases also showed a lower seizure risk. A WHO grade III was associated with the highest risk of seizures, followed by grade II, while there was no significant difference between grade I and IV tumors.

Seizure prevalence and seizure risk difference in relation to tumor topography is given in Figs. 2 and 3 and Table 2. While no right-left difference was seen, bilateral tumors were associated with a significantly reduced risk of seizures. Compared to 44.4% for supratentorial tumors, the risk of seizures for infratentorial tumors was significantly and substantially lower with 0.9%. No difference was found between tumors involving one or more cerebral lobes or one or more cerebral gyri. Tumors without the involvement of a cerebral lobe or gyrus, however, showed a profoundly reduced risk of seizures. Involvement of the central or insular lobes was associated with a significant and relevant increase in seizure risk. While the involvement of the frontal, temporal and limbic lobes was also associated with an increased risk of seizures, albeit to a lesser extent, no such association was observed with the parietal and occipital lobes. On a gyral level, an involvement of the posterior third of the superior and middle frontal gyrus, the adjacent precentral, postcentral and subcentral gyrus, as well as paracentral lobule proved to be epileptogenic. The same applies to the posterior orbital gyrus, the rectus gyrus and the subcallosal area. An involvement

Table 1
Seizure risk in relation to demographic and histopathologic characteristics. The demographic and histopathologic composition of our cohort is shown with the seizure risk and seizure risk difference (at the time of diagnosis), stratified by age, sex, histological entity and WHO grade. Wilson 95% confidence intervals were calculated for seizure prevalence and seizure risk difference. *Abbreviations:* NA: Not applicable (i.e. tumors which are not assigned a WHO grade, e.g. metastases), t/v = training dataset / validation dataset.

Feature		Affected			Seizure risk (95%CI)		*Seizure risk difference* (95%CI)
		n	%	t/v	n	%	
Total		923	100%	646/277	347	37.6%	–
Age							
	0–20	84	9.1%	63/21	16	19.0% (from 12.1 to 28.7)	REF
	21–40	106	11.5%	72/34	55	51.9% (from 42.5 to 61.2)	**32.9** (from 19.3 to 44.4)
	40–60	314	34.0%	224/90	131	41.7% (from 36.4 to 47.2)	**22.7** (from 11.6 to 31.6)
	>60	419	45.4%	287/132	145	34.6% (from 30.2 to 39.3)	**15.6** (from 4.9 to 23.9)
Gender							
	Male	547	59.3%	382/165	202	36.9% (from 33.0 to 41.1)	REF
	Female	376	40.7%	264/112	145	38.6% (from 33.8 to 43.6)	1.7 (from −4.7 to 8.0)
Histological entity							
	GBM	351	38.0%	240/111	146	41.6% (from 36.6 to 46.8)	REF
	Astrocytoma (diffuse or anaplastic)	92	10.0%	55/37	66	71.7% (from 61.8 to 79.9)	**30.1** (from 18.9 to 39.8)
	Oligoastrocytoma (diffuse or anaplastic)	21	2.3%	14/7	17	81.0% (from 60 to 92.3)	**39.4** (from 17.8 to 51.8)
	Oligodendroglioma (diffuse or anaplastic)	38	4.1%	27/11	21	55.3% (from 39.7 to 69.9)	13.7 (from −2.7 to 29.1)
	Pilocytic astrocytoma	29	3.1%	25/4	0	0% (from 0 to 11.7)	**−41.6** (from −46.8 to −28.9)
	Medulloblastoma	14	1.5%	10/4	0	0% (from 0 to 21.5)	**−41.6** (from −46.8 to −19.5)
	Ependymoma	26	2.8%	21/5	3	11.5% (from 4 to 29)	**−30.1** (from −39.2 to −11.9)
	Developmental (DNET & ganglioglioma)	18	2.0%	11/7	14	77.8% (from 54.8 to 91.0)	**36.2** (from 12.6 to 50.3)
	Miscellaneous neuroepithelial*	18	2.0%	13/5	2	11.1% (from 3.1 to 32.8)	**−30.5** (from −40.0 to −8.2)
	Primary CNS lymphoma	35	3.8%	19/16	9	25.7% (from 14.2 to 42.1)	−15.9 (from −28.6 to 1.2)
	Metastases	281	30.4%	211/70	69	24.6% (from 19.9 to 29.9)	**−17.0** (from −24.0 to −9.7)
WHO grade							
	WHO grade I	52	5.6%	41/11	15	28.8% (from 18.3 to 42.3)	REF
	WHO grade II	68	7.4%	50/18	34	50.0% (from 38.4 to 61.6)	**21.2** (from 3.4 to 36.8)
	WHO grade III	119	12.9%	73/46	74	62.2% (from 53.2 to 70.4)	**33.4** (from 17.2 to 46.7)
	WHO grade IV	367	39.8%	251/116	146	39.8% (from 34.9 to 44.9)	10.9 (from −3.3 to 22.6)
	WHO grade NA	317	34.3%	231/86	78	24.6% (from 20.2 to 29.6)	−4.2 (from −18.4 to 7.4)

***Miscellaneous neuroepithelial:** including AT/RT (atypical teratoid/rhabdoid tumor), central neurocytoma, pilomyxoid astrocytoma, PXA (pleomorphic xanthastrocytoma), plexus papilloma, PNET (primitive neuroectodermal tumor), RGNT (rosette forming glioneuronal tumor), SGCA (subependymal giant cell astrocytoma), subependymoma.

Table 2
Seizure risk in relation to tumor topography. The topographic anatomical distribution of tumors is shown with the associated seizure risk and seizure risk difference (seizure risk in patients where the anatomical structure was affected by the tumor minus seizure risk in patients where the anatomical structure was not affected by the tumor). *Abbreviations:* t/v = training dataset / validation dataset.

Involved structure	Affected			Seizure risk *affected* (95%CI)		Seizure risk *non-affected* (95% CI)		*Seizure risk difference* (95% CI)
	n	%	t/v	n	%	n	%	
SIDE								
Right	356	38.6%	239/117	153	43.0% (from 37.9 to 48.2)	–	–	REF
Left	346	37.5%	247/99	145	41.9% (from 36.8 to 47.2)	–	–	−1.1 (from −8.3 to 6.2)
Both	221	23.9%	160/61	49	22.2% (from 17.2 to 28.1)	–	–	**−20.8** (from −28.0 to −13.0)
RELATION TO TENTORIUM								
Supratentorial	745	80.7%	515/230	331	44.4% (from 40.9 to 48.0)	–	–	REF
Infratentorial	115	12.5%	84/31	1	0.9% (from 0.2 to 4.8)	–	–	**−43.5** (from −47.2 to −38.3)
Both	63	6.8%	47/16	15	23.8% (from 15.0 to 35.6)	–	–	**−20.6** (from −30.1 to −8.3)
SUPRATENTORIAL STRUCTURES								
Cerebral lobes								
Unilobar	529	57.3%	371/158	250	47.3% (from 43.0 to 51.5)	–	–	REF
Multilobar	217	23.5%	148/69	92	42.4% (from 36.0 to 49.0)	–	–	−4.9 (from −12.5 to 3.0)
No cerebral lobe affected (none)	177	19.2%	127/50	5	2.8% (from 1.2 to 6.4)	–	–	**−44.5** (from −49.0 to −38.9)
Frontal lobe	267	28.9%	185/92	119	44.6% (from 38.7 to 50.6)	228	34.8% (from 31.2 to 38.5)	**9.8** (from 2.9 to 16.8)
Central lobe	124	13.4%	84/40	76	61.3% (from 52.5 to 69.4)	271	33.9% (from 30.7 to 37.3)	**27.4** (from 18.0 to 36.1)
Parietal lobe	171	18.5%	116/55	71	41.5% (from 34.4 to 49.0)	276	36.7% (from 33.3 to 40.2)	4.8 (from −3.1 to 13)
Occipital lobe	123	13.3%	87/36	43	35.0% (from 27.1 to 43.7)	304	38.0% (from 34.7 to 41.4)	−3.0 (from −11.6 to 6.3)
Temporal lobe	204	22.1%	145/59	94	46.1% (from 39.4 to 52.9)	253	35.2% (from 31.8 to 38.7)	**10.9** (from 3.3 to 18.5)
Insular lobe	59	6.4%	38/21	38	64.4% (from 51.7 to 75.4)	309	35.8% (from 32.6 to 39.0)	**28.6** (from 15.5 to 40.1)
Limbic lobe	133	14.4%	92/41	61	45.9% (from 37.6 to 54.3)	286	36.2% (from 32.9 to 39.6)	**9.7** (from 0.8 to 18.7)
Cerebral gyral segments								
Unigyral	447	48.4%	316/131	208	46.5% (from 42.0 to 51.2)	–	–	**REF**
Multigyral	297	32.2%	201/96	133	44.8% (from 39.2 to 50.5)	–	–	−1.7 (from −9.0 to 5.5)
No cerebral gyral segment affected	179	19.4%	129/50	6	3.4% (from 1.5 to 7.1)	–	–	**−43.2** (from −48.2 to −37.2)
Frontal pole	16	1.73%	12/4	5	31.2% (from 14.2 to 55.6)	342	37.7% (from 34.6 to 40.9)	−6.5 (from −23.8 to 18.1)
Anterior superior frontal gyrus (anterior third)	56	6.07%	40/16	22	39.3% (from 27.6 to 52.4)	325	37.5% (from 34.3 to 40.8)	1.8 (from −10.4 to 15.3)
Middle superior frontal gyrus (middle third)	52	5.63%	38/14	24	46.2% (from 33.3 to 59.5)	323	37.1% (from 33.9 to 40.3)	9.1 (-4.2 to 22.8)
Posterior superior frontal gyrus (posterior third)	75	8.13%	50/25	43	57.3% (from 46.1 to 67.9)	304	35.8% (from 32.7 to 39.1)	**21.5** (from 9.7 to 32.5)
Anterior middle frontal gyrus (anterior third)	58	6.28%	36/22	21	36.2% (from 25.1 to 49.1)	326	37.7% (from 34.5 to 41.0)	−1.5 (from −13.1 to 11.8)
Middle middle frontal gyrus (middle third)	49	5.31%	34/15	16	32.7% (from 21.2 to 46.6)	331	37.9% (from 34.7 to 41.1)	−5.2 (from −17.1 to 9.1)
Posterior middle frontal gyrus (posterior third)	59	6.39%	36/23	33	55.9% (from 43.3 to 67.8)	314	36.3% (from 33.2 to 39.6)	**19.6** (from 6.5 to 31.9)
Inferior frontal gyrus, orbital part	27	2.93%	19/8	10	37.0% (from 21.5 to 55.8)	337	37.6% (from 34.5 to 40.8)	−0.6 (from −16.4 to 18.4)
Inferior frontal gyrus, triangular part	34	3.68%	22/12	14	41.2% (from 26.4 to 57.8)	333	37.5% (from 34.3 to 40.7)	3.7 (from −11.4 to 20.6)
Inferior frontal gyrus, opercular part	37	4.01%	22/15	18	48.6% (from 33.4 to 64.1)	329	37.1% (from 34.0 to 40.4)	11.5 (from −4 to 27.3)
Anterior orbital gyrus	10	1.08%	6/4	4	40.0% (from 16.8 to 68.7)	343	37.6% (from 34.5 to 40.8)	2.4 (from −21.0 to 31.3)
Medial orbital gyrus	16	1.73%	10/6	9	56.2% (from 33.2 to 76.9)	338	37.3% (from 34.2 to 40.5)	19.0 (from −4.3 to 39.9)
Lateral orbital gyrus	14	1.52%	10/4	4		343		−9.1 (from −26.3 to 17.1)

(*continued on next page*)

Table 2 (*continued*)

Involved structure	Affected			Seizure risk *affected* (95%CI)		Seizure risk *non-affected* (95% CI)		*Seizure risk difference* (95% CI)
	n	%	t/v	n	%	n	%	
					28.6% (from 11.7 to 54.6)		37.7% (from 34.6 to 40.9)	
Posterior orbital gyrus	32	3.47%	18/14	18	56.2% (from 39.3 to 71.8)	329	36.9% (from 33.8 to 40.1)	**19.3** (from 2.1 to 35.2)
Gyrus rectus	15	1.63%	6/9	10	66.7% (from 41.7 to 84.8)	337	37.1% (from 34.0 to 40.3)	**29.6** (from 4.4 to 48.0)
Rostral gyrus	13	1.41%	6/7	6	46.2% (from 23.2 to 70.9)	341	37.5% (from 34.4 to 40.7)	8.7 (from −14.5 to 33.6)
Subcallosal area	20	2.17%	11/9	12	60.0% (from 38.7 to 78.1)	335	37.1% (from 34.0 to 40.3)	**22.9** (from 1.3 to 41.3)
Precentral gyrus	57	6.18%	39/18	29	50.9% (from 38.3 to 63.4)	318	36.7% (from 33.6 to 40.0)	**14.2** (from 1.1 to 27.1)
Postcentral gyrus	46	4.98%	31/15	29	63.0% (from 48.6 to 75.5)	318	36.3% (from 33.1 to 39.5)	**26.8** (from 12.0 to 39.6)
Paracentral lobule	29	3.14%	19/10	18	62.1% (from 44.0 to 77.3)	329	36.8% (from 33.7 to 40.0)	**25.3** (from 6.9 to 40.8)
Subcentral gyrus	34	3.68%	22/12	19	55.9% (from 39.5 to 71.1)	328	36.9% (from 33.8 to 40.1)	**19.0** (from 2.2 to 34.5)
Superior parietal lobule	41	4.44%	30/11	19	46.3% (from 32.1 to 61.3)	328	37.2% (from 34.1 to 40.4)	9.2 (from −5.5 to 24.4)
Supramarginal gyrus	67	7.26%	45/22	30	44.8% (from 33.5 to 56.6)	317	37.0% (from 33.9 to 40.3)	7.8 (from −4.0 to 20.0)
Angular gyrus	47	5.09%	30/17	20	42.6% (from 29.5 to 56.7)	327	37.3% (from 34.2 to 40.6)	5.2 (from −8.2 to 19.7)
Precuneus	58	6.28%	38/20	22	37.9% (from 26.6 to 50.8)	325	37.6% (from 34.4 to 40.8)	0.4 (from −11.5 to 13.6)
Cuneus	37	4.01%	27/10	13	35.1% (from 21.8 to 51.2)	334	37.7% (from 34.6 to 40.9)	−2.6 (from −16.3 to 13.8)
Superior occipital gyrus	22	2.38%	17/5	6	27.3% (from 13.2 to 48.2)	341	37.8% (from 34.7 to 41.1)	−10.6 (from −25.1 to 10.5)
Middle occipital gyrus	50	5.42%	38/12	17	34.0% (from 22.4 to 47.8)	330	37.8% (from 34.6 to 41.1)	−3.8 (from −15.8 to 10.4)
Inferior occipital gyrus	19	2.06%	14/5	6	31.6% (from 15.4 to 54.0)	341	37.7% (from 34.6 to 40.9)	−6.1 (from −22.7 to 16.5)
Occipital pole	3	0.33%	2/1	0	0% (from 0 to 56.1)	347	37.7% (from 34.6 to 40.9)	−37.7 (from −40.9 to 18.5)
Lingual gyrus	29	3.14%	22/7	15	51.7% (from 34.4 to 68.6)	332	37.1% (from 34.0 to 40.4)	14.6 (from −3.0 to 31.8)
Fusiform gyrus	47	5.09%	33/14	21	44.7% (from 31.4 to 58.8)	326	37.2% (from 34.1 to 40.5)	7.5 (from −6.2 to 21.9)
Anterior superior temporal gyrus (anterior third)	42	4.55%	25/17	21	50.0% (from 35.5 to 64.5)	326	37.0% (from 33.9 to 40.2)	13.0 (from −1.8 to 27.8)
Middle superior temporal gyrus (middle third)	34	3.68%	22/12	16	47.1% (from 31.5 to 63.3)	331	37.2% (from 34.1 to 40.5)	9.9 (from −6.1 to 26.3)
Posterior superior temporal gyrus (posterior third)	40	4.33%	27/13	16	40.0% (from 26.3 to 55.4)	331	37.5% (from 34.4 to 40.7)	2.5 (from −11.5 to 18.2)
Anterior middle temporal gyrus (anterior third)	38	4.12%	27/11	18	47.4% (from 32.5 to 62.7)	329	37.2% (from 34.1 to 40.4)	10.2 (from −5.0 to 25.9)
Middle middle temporal gyrus (middle third)	35	3.79%	28/7	18	51.4% (from 35.6 to 67.0)	329	37.0% (from 33.9 to 40.3)	14.4 (from −1.8 to 30.3)
Posterior middle temporal gyrus (posterior third)	38	4.12%	28/10	20	52.6% (from 37.3 to 67.5)	327	36.9% (from 33.8 to 40.2)	15.7 (from 0.0 to 30.9)
Anterior inferior temporal gyrus (anterior third)	27	2.93%	26/9	19	70.4% (from 51.5 to 84.1)	328	36.6% (from 33.5 to 39.8)	**33.5** (from 14.6 to 47.9)
Middle inferior temporal gyrus (middle third)	35	3.79%	20/7	15	42.9% (from 28.0 to 59.1)	332	37.4% (from 34.3 to 40.6)	5.5 (from −9.7 to 22.1)
Posterior inferior temporal gyrus (posterior third)	33	3.58%	26/7	15	45.5% (from 29.8 to 62.0)	332	37.3% (from 34.2 to 40.5)	8.2 (from −7.8 to 25)
Planum temporale	7	0.76%	6/1	2	28.6% (from 8.2 to 64.1)	345	37.7% (from 34.6 to 40.8)	−9.1 (from −29.7 to 26.6)
Planum polare	21	2.28%	15/6	11	52.4% (from 32.4 to 71.7)	336	37.3% (from 34.2 to 40.5)	15.1 (from −5.1 to 34.7)
Temporal pole	44	4.77%	26/18	28	63.6% (from 48.9 to 76.2)	319	36.3% (from 33.2 to 39.5)	**27.3** (from 12.2 to 40.3)
Short insular gyri	49	5.31%	31/18	31	63.3% (from 49.3 to 75.3)	316	36.2% (from 33.0 to 39.4)	**27.1** (from 12.7 to 39.6)
Long insular gyri	45	4.88%	29/16	29	64.4% (from 49.8 to 76.8)	318	36.2% (from 33.1 to 39.5)	**28.2** (from 13.3 to 40.9)
Parahippocampal gyrus	48	5.2%	31/17	29	60.4% (from 46.3 to 73.0)	318	36.3% (from 33.2 to 39.6)	**24.1** (from 9.6 to 37.0)
Anterior cingulate gyrus (anterior third)	39	4.23%	29/10	19	48.7% (from 33.9 to 63.8)	328	37.1% (from 34.0 to 40.3)	11.6 (from −3.6 to 27.0)
Middle cingulate gyrus (middle third)	33	3.58%	26/7	17		330		14.4 (from −2.2 to 30.7)

(*continued on next page*)

Table 2 (*continued*)

Involved structure	Affected			Seizure risk *affected* (95%CI)		Seizure risk *non-affected* (95% CI)		*Seizure risk difference* (95% CI)
	n	%	t/v	n	%	n	%	
					51.5% (from 35.2 to 67.5)		37.1% (from 34.0 to 40.3)	
Posterior cingulate gyrus (posterior third)	36	3.9%	24/12	14	38.9% (from 24.8 to 55.1)	333	37.5% (from 34.4 to 40.8)	1.4 (from −13.1 to 17.9)
Cerebral cortex	713	77.25%	496/217	331	46.4% (from 42.8 to 50.1)	16	7.6% (from 4.7 to 12.0)	**38.8** (from 33.1 to 43.5)
Cerebral peripheral white matter	734	79.52%	512/222	329	44.8% (from 41.3 to 48.4)	18	9.5% (from 6.1 to 14.6)	**35.3** (from 29.1 to 40.3)
Subcortical white matter (sector 1)	713	77.25%	496/217	324	45.4% (from 41.8 to 49.1)	23	11% (from 7.4 to 15.9)	**34.5** (from 28.4 to 39.6)
Subgyral white matter (sector 2)	649	70.31%	449/200	292	45.0% (from 41.2 to 48.8)	55	20.1% (from 15.8 to 25.2)	**24.9** (from 18.5 to 30.7)
Gyral white matter (sector 3)	540	58.5%	372/168	254	47.0% (from 42.9 to 51.3)	93	24.3% (from 20.3 to 28.8)	**22.7** (from 16.6 to 28.6)
Lobar white matter (sector 4)	462	50.05%	315/147	213	46.1% (from 41.6 to 50.7)	134	29.1% (from 25.1 to 33.4)	**17.0** (from 10.8 to 23.1)
Corpus callosum	99	10.73%		31	31.3% (from 23.0 to 41.0)	316	38.3% (from 5.1 to 41.7)	−7.0 (from −16 to 3.2)
Central involvement	34	3.68%	22/12	6	17.6% (from 8.3 to 33.5)	341	38.4% (from 35.2 to 41.6)	**−20.8** (from −30.6 to −4.5)
Marginal involvement: subependymal	89	9.64%	62/27	30	33.7% (from 24.7 to 44.0)	317	38.0% (from 34.8 to 41.4)	−4.3 (from −13.9 to 6.5)
Marginal involvement: subpial	30	3.25%	21/9	6	20.0% (from 9.5 to 37.3)	341	38.2% (from 35.1 to 41.4)	**−18.2** (from −29.2 to −0.6)
Cerebral central gray matter								
Caudate nucleus	14	1.52%	11/3	4	28.6% (from 11.7 to 54.6)	343	37.7% (from 34.7 to 40.9)	−9.1 (from −26.3 to 17.1)
Putamen	11	1.19%	8/3	3	27.3% (from 9.7 to 56.6)	344	37.7% (from 34.6 to 40.9)	−10.4 (from −28.3 to 19.0)
Globus pallidus	11	1.19%	8/3	4	36.4% (from 15.2 to 64.6)	343	37.6% (from 34.5 to 40.8)	−1.2 (from −22.7 to 27.2)
Claustrum	27	2.93%	16/11	14	51.9% (from 34.0 to 69.3)	333	37.2% (from 34.1 to 40.4)	14.7 (from −3.5 to 32.4)
Hypothalamus	21	2.28%	16/5	6	28.6% (from 13.8 to 50.0)	341	37.8% (from 34.7 to 41.0)	−9.2 (from −24.3 to 12.4)
Amygdala	44	4.77%	28/16	29	65.9% (from 51.1 to 78.1)	318	36.2% (from 33.1 to 39.4)	**29.7** (from 14.6 to 42.3)
Hippocampus	56	6.07%	38/18	34	60.7% (from 47.6 to 72.4)	313	36.1% (from 33.0 to 39.4)	**24.6** (from 11.1 to 36.7)
Thalamus	47	5.09%	31/16	13	27.7% (from 16.9 to 41.8)	334	38.1% (from 35.0 to 41.4)	−10.5 (from −21.7 to 4.0)
Cerebral central white matter								
Internal capsule	14	1.52%	11/3	4	28.6% (from 11.7 to 54.6)	343	37.7% (from 34.6 to 40.9)	−9.1 (from −26.3 to 17.1)
External capsule	34	3.68%	21/13	19	55.9% (from 39.5 to 71.1)	328	36.9% (from 33.8 to 40.1)	**19.0** (from 2.2 to 34.5)
Extreme capsule	37	4.01%	22/15	20	54.1% (from 38.4 to 69.0)	327	36.9% (from 33.8 to 40.1)	**17.1** (from 1.1 to 32.4)
Innominate substance	39	4.23%	25/14	20	51.3% (from 36.2 to 66.1)	327	37.0% (from 33.9 to 40.2)	14.3 (from −1.1 to 29.5)
Ventricular wall	521	56.45%		228	43.8% (from 39.6 to 48.1)	119	29.6% (from 25.3 to 34.2)	**14.2** (from 7.9 to 20.2)
Focal	163	17.66%	118/45	95	58.3% (from 50.6 to 65.6)	–	–	REF
Diffuse	358	38.79%	243/124	133	37.2% (from 32.3 to 42.3)	–	–	**−21.1** (from −29.9 to −11.9)
Lateral ventricle								
Frontal horn of lateral ventricle	165	17.88%	112/53	69	41.8% (from 34.6 to 49.4)	278	36.7% (from 33.3 to 40.2)	5.1 (from −2.9 to 13.5)
Body of lateral ventricle	129	13.98%	81/48	58	45.0% (from 36.6 to 53.6)	289	36.4% (from 33.1 to 39.8)	8.6 (from −0.4 to 17.8)
Atrium of lateral ventricle	241	26.11%	163/78	100	41.5% (from 35.5 to 47.8)	247	36.2% (from 32.7 to 39.9)	5.3 (from −1.8 to 12.5)
Occipital horn of lateral ventricle	83	8.99%	61/22	29	34.9% (from 25.6 to 45.7)	318	37.9% (from 34.6 to 41.2)	−3.0 (from −12.9 to 8.3)
Temporal horn of lateral ventricle	157	17.01%	104/53	69	43.9% (from 36.4 to 51.8)	278	36.3% (from 33.0 to 39.8)	7.6 (from −0.6 to 16.2)
Third ventricle	35	3.79%	22/13	8	22.9% (from 12.1 to 39.0)	339	38.2% (from 35.0 to 41.4)	−15.3 (from −26.6 to 1.1)
Aqueduct	15	1.63%	9/6	2	13.3% (from 3.7 to 37.9)	345	38.0% (from 34.9 to 41.2)	−24.7 (from −34.8 to 0.1)
Fourth ventricle								

(*continued on next page*)

Table 2 (*continued*)

Involved structure	Affected			Seizure risk *affected* (95%CI)		Seizure risk *non-affected* (95% CI)		*Seizure risk difference* (95% CI)
	n	%	t/v	n	%	n	%	
Fourth ventricle: Superior (apex)	11	1.19%	5/6	3	27.3% (from 9.7 to 56.6)	344	37.7% (from 34.6 to 40.9)	−10.4 (from −28.3 to 19.0)
Fourth ventricle: lateral (recess)	65	7.04%	47/18	3	4.6% (from 1.6 to 12.7)	344	40.1% (from 36.9 to 43.4)	**−35.5** (from −40.0 to −26.8)
Fourth ventricle: inferior (obex)	16	1.73%	7/9	1	6.2% (from 1.1 to 28.3)	346	38.1% (from 35.0 to 41.4)	**−31.9** (from −38.0 to −9.6)
Fourth ventricle: dorsal (fastigium)	21	2.28%	13/8	2	9.5% (from 2.7 to 28.9)	345	38.2% (from 35.1 to 41.5)	**−28.7** (from −36.3 to −9.1)
Septum pellucidum	20	2.17%	11/9	1	5.0% (from 0.9 to 23.6)	346	38.3% (from 35.2 to 41.5)	−33.3 (from −38.5 to 14.4)
Choroid plexus of lateral ventricle	8	0.87%	6/2	1	12.5% (from 2.2 to 47.1)	346	37.8% (from 34.7 to 41.0)	−25.3 (from −36.1 to 9.4)
Supratentorial leptomeninges	47	5.09%	32/15	18	38.3% (from 25.8 to 52.6)	329	37.6% (from 34.4 to 40.8)	0.7 (from −12.2 to 15.4)
INFRATENTORIAL STRUCTURES								
Brainstem								
Mesencephalon (tectum)	4	0.43%	1/2	0	0% (from 0.0 to 49.0)	347	37.8% (from 34.7 to 40.9)	−37.8 (from −40.9 to 11.3)
Mesencephalon (tegmentum)	2	0.22%	2/0	1	50.0% (from 9.5 to 90.5)	346	37.6% (from 34.5 to 40.7)	12.4 (from −28.2 to 53.1)
Mesencephalon (crus)	5	0.54%	5/0	0	0% (from 0.0 to 43.4)	347	37.8% (from 34.7 to 41.0)	−37.8 (from −41.0 to 5.8)
Mesencephalon (subpial)	4	0.43%	3/1	0	0% (from 0.0 to 49.0)	347	37.8% (from 34.7 to 40.9)	−37.8 (from −40.9 to 11.3)
Pons (tegmentum)	23	2.49%	17/6	0	0% (from 0.0 to 14.3)	347	38.6% (from 35.4 to 41.8)	**−38.6** (from −41.8 to –23.9)
Pons (base)	12	1.3%	10/2	0	0% (from 0.0 to 24.2)	347	38.1% (from 35.0 to 41.3)	**−38.1** (from −41.3 to −13.6)
Pons (subpial)	4	0.43%	3/1	0	0% (from 0.0 to 49.0)	347	37.8% (from 34.7 to 40.9)	−37.8 (from −40.9 to 11.3)
Medulla oblongata (tegmentum)	9	0.98%	5/4	0	0% (from 0.0 to 29.9)	347	38.0% (from 34.9 to 41.2)	**−38.0** (from −41.2 to −7.9)
Medulla oblongata (base)	5	0.54%	3/2	0	0% (from 0.0 to 43.4)	347	37.8% (from 34.7 to 41.0)	−37.8 (from −41.0 to 5.8)
Medulla oblongata (subpial)	3	0.33%	3/0	0	0% (from 0.0 to 56.1)	347	37.7% (from 34.6 to 40.9)	−37.7 (from −40.9 to 18.5)
Cerebellar lobes								
Anterior cerebellar lobe	29	3.14%	18/11	2	6.9% (from 1.9 to 22.0)	345	38.6% (from 35.5 to 41.8)	**−31.7** (from −37.6 to −16.3)
Middle cerebellar lobe	35	3.79%	29/6	4	11.4% (from 4.5 to 26.0)	343	38.6% (from 35.5 to 41.9)	**−27.2** (from −34.8 to −12.3)
Posterior cerebellar lobe	81	8.78%	65/16	8	9.9% (from 5.1 to 18.3)	339	40.3% (from 37.0 to 43.6)	**−30.4** (from −26.2 to −21.4)
Flocculonodular cerebellar lobe	16	1.73%	13/3	0	0% (from 0.0 to 19.4)	347	38.3% (from 35.2 to 41.5)	**−38.3** (from −41.5 to −18.6)
Cerebellar vermian lobules								
Central	12	1.3%	9/3	0	0% (from 0.0 to 24.2)	347	38.1% (from 35.0 to 41.3)	**−38.1** (from −41.3 to −13.6)
Culmen	13	1.41%	9/4	0	0% (from 0.0 to 22.8)	347	38.1% (from 35.0 to 41.3)	**−38.1** (from −41.3 to −15.1)
Declive	11	1.19%	9/2	0	0% (from 0.0 to 25.9)	347	38.0% (from 35.0 to 41.2)	**−38.0** (from −41.2 to −12.0)
Folium	9	0.98%	8/1	0	0% (from 0.0 to 29.9)	347	38.0% (from 34.9 to 41.2)	**−38.0** (from −41.2 to −7.9)
Tuber	8	0.87%	8/0	0	0% (from 0.0 to 32.4)	347	37.9% (from 34.8 to 41.1)	**−37.9** (from −41.1 to −5.3)
Pyramid	7	0.76%	6/1	0	0% (from 0.0 to 35.4)	347	37.9% (from 34.8 to 41.1)	**−37.9** (from −41.1 to −2.3)
Uvula	10	1.08%	8/2	0	0% (from 0.0 to 27.8)	347	38.0% (from 34.9 to 41.2)	**−38.0** (from −41.2 to −10.1)
Nodule	15	1.63%	12/3	0	0% (from 0.0 to 20.4)	347	38.2% (from 35.1 to 41.4)	**−38.2** (from −41.4 to −17.6)
Cerebellar hemispheric lobules								
Ala lobuli centralis	10	1.08%	8/2	1	10% (from 1.8 to 40.4)	346	37.9% (from 34.8 to 41.1)	−27.9 (from −36.7 to 2.7)
Anterior quadrangular lobule	18	1.95%	13/5	0	0% (from 0.0 to 17.6)	347	38.3% (from 35.2 to 41.6)	**−38.3** (from −41.6 to −20.5)
Posterior quadrangular lobule	13	1.41%	11/2	2	15.4% (from 4.3 to 42.2)	345	37.9% (from 34.8 to 41.1)	–22.5 (from −34.0 to 4.5)
Superior semilunar lobule	29	3.14%	24/5	3	10.3% (from 3.6 to 26.4)	344	38.5% (from 35.3 to 41.7)	**−28.1** (from −35.6 to –11.8)
Inferior semilunar / gracile lobule	53	5.74%	46/7	5	9.4% (from 4.1 to 20.3)	342		

(*continued on next page*)

Table 2 (*continued*)

Involved structure	Affected			Seizure risk *affected* (95%CI)		Seizure risk *non-affected* (95% CI)		*Seizure risk difference* (95% CI)
	n	%	t/v	n	%	n	%	
							39.3% (from 36.1 to 42.6)	**−29.9** (from −36.1 to −18.6)
Biventer lobule	25	2.71%	18/7	1	4.0% (from 0.7 to 19.5)	346	38.5% (from 35.4 to 41.8)	**−34.5** (from −39.1 to −18.7)
Tonsilla	10	1.08%	10/0	2	20.0% (from 5.7 to 51.0)	345	37.8% (from 34.7 to 41.0)	−17.8 (from −32.5 to 13.3)
Flocculus	6	0.65%	6/0	0	0% (from 0.0 to 39.0)	347	37.8% (from 34.8 to 41.0)	−37.8 (from −41.0 to 1.3)
Cerebellar cortex	121	13.11%	90/31	11	9.1% (from 5.2 to 15.5)	336	41.9% (from 38.5 to 45.3)	**−32.8** (from −38.0 to −25.5)
Cerebellar peripheral white matter	120	13.0%	89/31	11	9.2% (from 5.2 to 15.7)	336	41.8% (from 38.5 to 45.3)	**−32.6** (from −37.9 to −25.4)
Subcortical white matter (sector 1)	120	13.0%	89/31	11	9.2% (from 5.2 to 15.7)	336	41.8% (from 38.5 to 45.3)	**−32.6** (from −37.9 to −25.4)
Sublobular white matter (sector 2)	108	11.7%	78/30	5	4.6% (from 2.0 to 10.4)	342	42.0% (from 38.6 to 45.4)	**−37.4** (from −41.7 to −30.7)
Lobular white matter (sector 3)	88	9.53%	66/22	3	3.4% (from 1.2 to 9.5)	344	41.2% (from 37.9 to 44.6)	**−37.8** (from −41.8 to −30.8)
Lobar white matter (sector 4)	43	4.66%	34/9	0	0% (from 0.0 to 8.2)	347	39.4% (from 36.3 to 42.7)	**−39.4** (from −42.7 to −30.6)
Cerebellar nuclei	11	1.19%	9/2	0	0% (from 0.0 to 25.9)	347	38% (from 35.0 to 41.2)	**−38.0** (from −41.2 to −12.0)
Cerebellar peduncles								
Superior cerebellar peduncle	8	0.87%	7/1	1	12.5% (from 2.2 to 47.1)	346	37.8% (from 34.7 to 41.0)	−25.3 (from −36.1 to 9.4)
Middle cerebellar peduncle	18	1.95%	12/6	0	0% (from 0.0 to 17.6)	347	38.3% (from 35.2 to 41.6)	**−38.3** (from −41.6 to −20.5)
Inferior cerebellar peduncle	8	0.87%	5/3	0	0% (from 0.0 to 32.4)	347	37.9% (from 34.8 to 41.1)	**−37.9** (from −41.1 to −5.3)
Infratentorial leptomeninges	24	2.60%	16/8	1	4.2% (from 0.7 to 20.2)	346	38.5% (from 35.4 to 41.7)	**−34.3** (from −39.0 to −17.9)

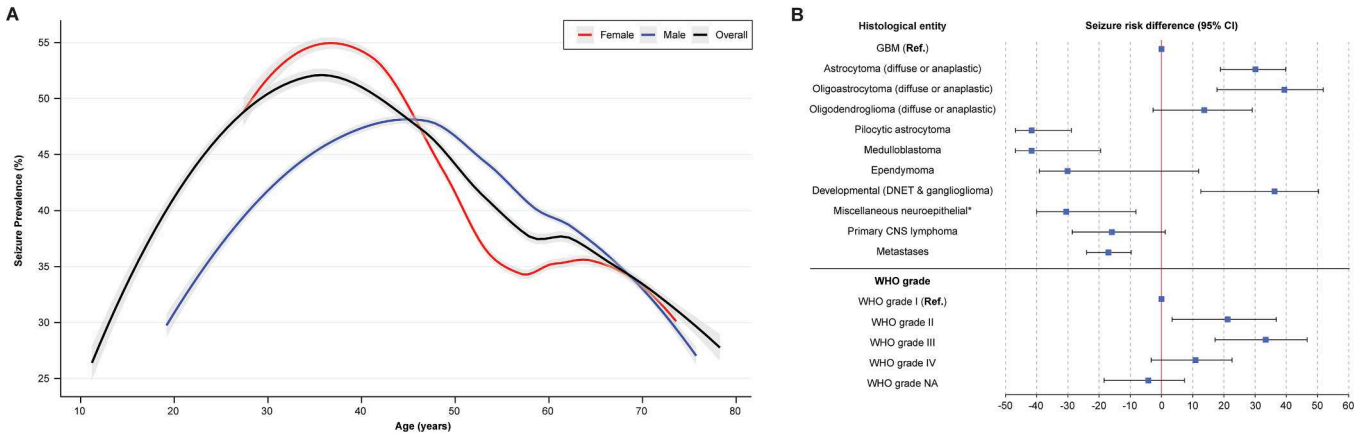

Fig. 1. Seizure risk dependent on demographic characteristics The risk of epileptic seizures is presented in relation to demographic characteristics. Fig. 1A: Seizure prevalence by age and gender. Fig. 1B: The influence of histopathologic tumor characteristics (histological entity and WHO grade) on seizure risk, defined as seizure risk difference in relation to the designated reference category (Ref.) with the corresponding 95% confidence interval (Wilson).

of the anterior third of the inferior temporal gyrus, the temporal pole, the short and long insular gyri and the parahippocampal gyrus was also associated with an increased seizure risk. An increased risk of seizures was furthermore found with the extreme and external capsule located underneath the insula. The involvement of the cerebral cortex proved to be a significant epileptic driver. Along the cortico-ventricular axis, epileptogenicity decreases gradually down the white matter sectors. While a subependymal involvement of the corpus callosum had no relevant effect on the seizure risk, a central and subpial affection of the corpus callosum showed a significantly reduced risk. Both the involvement of the amygdala and the hippocampus proved pro-epileptogenic. Diffuse involvement of the ventricular wall showed a reduced seizure risk compared to a focal involvement. All infratentorial brainstem or cerebellar structures were associated with a reduced risk of seizures.

4.1. Machine learning model

Results of the out-of-the-box preliminary investigation of model performance are given in Supplementary Table 5. Due to comparable performance to the other ML methods and the advantage of allowing the explanation of model-internal variable weighting through calculation of PD values, GAM was selected as the final model. The performance of the T, TD and TDH GAM are given in Table 3 and Fig. 4. Best performance at internal validation is seen with the TDH model (AUC: 0.79 (0.74–0.77), Accuracy: 0.72 (0.66–0.78), Sensitivity: 0.81 (0.74–0.88), Specificity: 0.66 (0.59–0.73)). Topographic features contribute the most to model

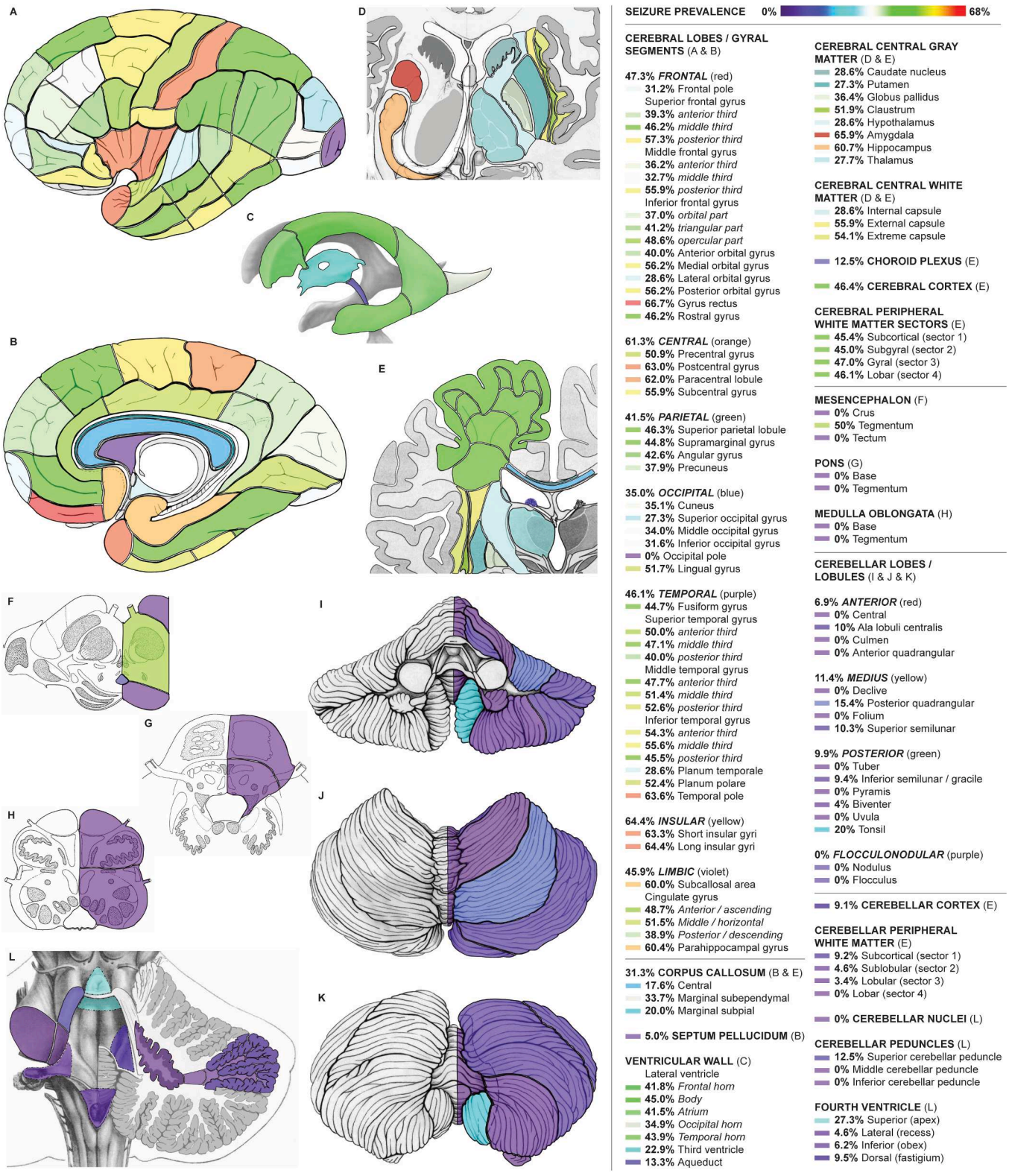

Fig. 2. Seizure prevalence in relation to tumor topography A color-coded representation of the prevalence of epileptic seizures at the time of diagnosis is shown, depending on the topographic anatomical structure involved by the tumor. Fig. 2A: Lateral view on the cerebral hemisphere with its gyral segments. Fig. 2B: Medial view on the cerebral hemisphere. Fig. 2C: Supratentorial ventricular walls. Fig. 2D: Supratentorial central white and gray matter. Fig. 2E: Coronal section through the cerebral hemisphere with the white matter sectors, the corpus callosum and the deep white and gray matter shown. Fig. 2F: Axial section through the mesencephalon. Fig. 2G: Axial section through the pons. Fig. 2H: Axial section through the medulla oblongata. Fig. 2I: Anterior view on the cerebellum with its vermian and hemispheric lobules. Fig. 2J: Superior view on the cerebellum. Fig. 2K: Inferior view on the cerebellum. Fig. 2L: Posterior view on the fourth ventricle, the cerebellar peduncles and the transected cerebellum with its white matter sectors and deep nuclei.

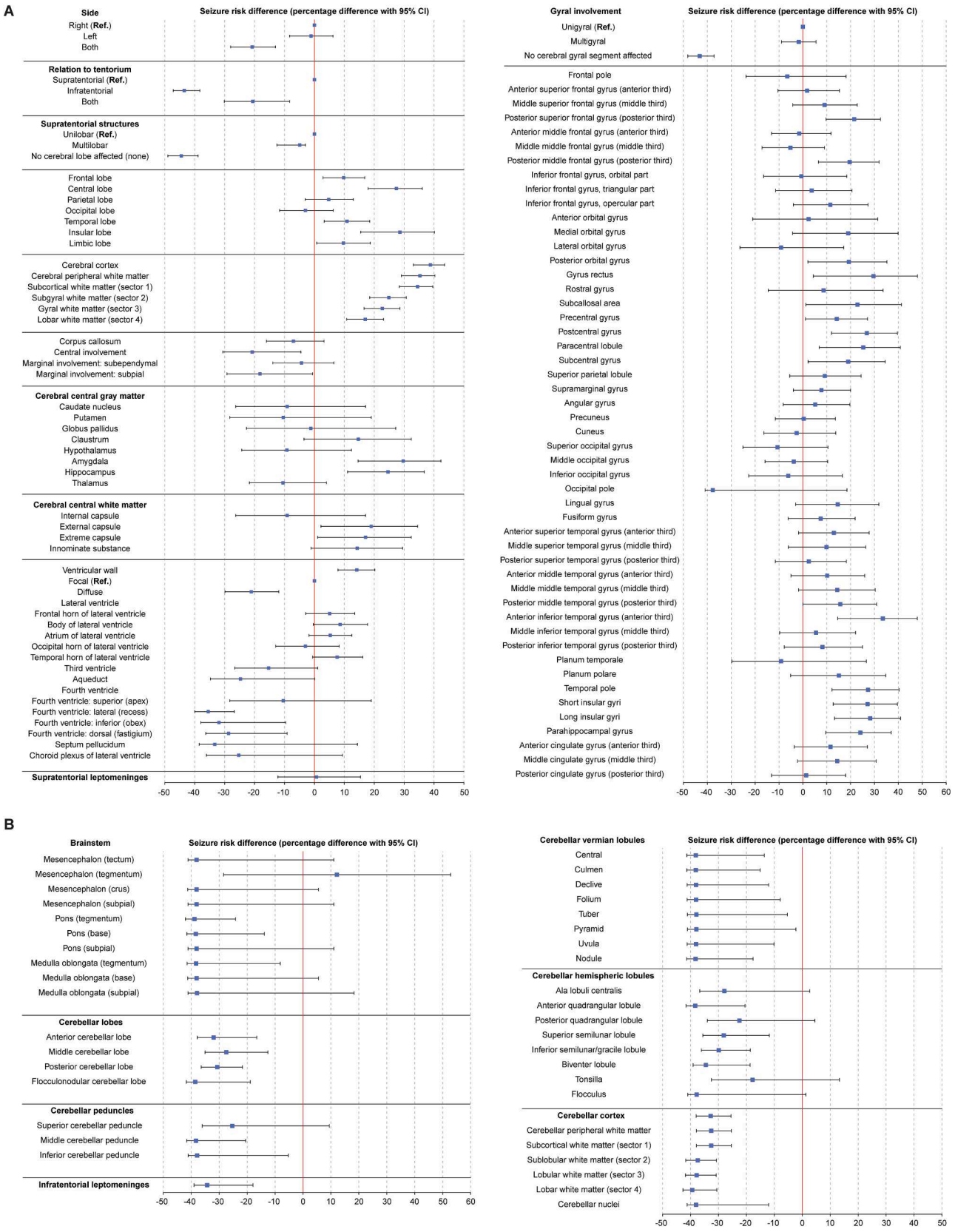

Fig. 3. Seizure risk dependent on topographic tumor anatomy. The influence of the tumor's involvement of specific topographic anatomical structures on seizure risk is shown. Binary factors are presented with their corresponding seizure risk difference (percentage difference: seizure risk if structure is affected minus seizure risk if structure is not affected), with a 95% confidence interval (Wilson confidence interval for risk differences). For categorical data with more than two levels, the seizure risk difference is given in relation to the designated reference (Ref.) with the corresponding 95% confidence interval (Wilson). Fig. 3A: General topographic anatomical categories and supratentorial anatomical structures. Fig. 3B: Infratentorial anatomical structures.

Table 3
Discrimination and calibration of the generalized additive models Performance measures of the topographic (T), topographic/demographic (TD) and topographic/demographic/histopathologic (TDH) generalized additive models after variables selection by recursive feature elimination at bootstrap on the train set and internal validation on a separate test set. AUC, Accuracy, Sensitivity, Specificity, PPV, NPV, F1 score, calibration curve intercept and slope with the corresponding 95% confidence intervals are reported. *Abbreviations:* AUC: area under the curve; PPV: positive predictive values; NPV: negative predictive value; T: topographic; TD: topographic/demographic; TDH: topographic/demographic/histopathologic.

Generalized additive models		T model		TD model		TDH model	
		Bootstrap	Validation	Bootstrap	Validation	Bootstrap	Validation
Discrimination	AUC	0.72 (0.70–0.73)	0.70 (0.64 to 0.76)	0.72 (0.71–0.74)	0.70 (0.63–0-76)	0.75 (0.74–0.77)	0.79 (0.74–0.84)
	Accuracy	0.65 (0.64–0.66)	0.64 (0.58–0.70)	0.66 (0.65–0.68)	0.66 (0.61–0.72)	0.69 (0.68–0.71)	0.72 (0.66–0.78)
	Sensitivity	0.62 (0.59–0.64)	0.66 (0.58 to 0.75)	0.65 (0.63–0.67)	0.68 (0.59–0.77)	0.71 (0.69–0.73)	0.81 (0.74–0.88)
	Specificity	0.68 (0.66–0.69)	0.63 (0.55 to 0.70)	0.67 (0.66–0.69)	0.65 (0.58–0.72)	0.69 (0.67–0.70)	0.66 (0.59–0.73)
	PPV	0.52 (0.50–0.54)	0.54 (0.45–0.63)	0.53 (0.52–0.55)	0.55 (0.47–0.63)	0.56 (0.54–0.58)	0.62 (0.53–0.70)
	NPV	0.76 (0.74–0.77)	0.73 (0.66–0.80)	0.77 (0.75–0.78)	0.77 (0.69–0.83)	0.81 (0.79–0.82)	0.84 (0.78–0.90)
	F1 score*	0.57	0.68	0.58	0.70	0.63	0.74
Calibration	Intercept	−0.52 (−0.71 to −0.34)	−0.42 (−0.70 to −0.15)	−0.49 (−0.68 to −0.31)	−0.41 (−0.70 to −0.12)	−0.48 (−0.68 to −0.28)	−0.47 (−0.77 to −0.17)
	Slope	0.92 (0.72 to 1.12)	0.52 (0.32 to 0.72)	0.94 (0.76 to 1.12)	0.46 (0.29 to 0.64)	0.94 (0.77 to 1.2)	0.57 (0.39 to 0.76)

* The F1 score is a composite score and represents the harmonic mean of precision (i.e. PPV) and sensitivity.

performance. The results of the PD and delta PD analysis of the TDH GAM are given in Fig. 5 and Supplementary Table 6. The highest positive delta partial dependence of the model is on the presence of an involvement of the cerebral cortex. The highest negative partial dependence is found with the involvement of the cerebellar lobular white matter and the cerebellar cortex.

5. Discussion

Aiming to identify clinically relevant risk factors for epileptic seizures in previously seizure free patients with brain tumors, the present study highlights the relevance of the topographic anatomical tumor characteristics and identifies specific phylogenetic anatomical patterns as epileptic drivers. Using a GAM, the seizure risk can be predicted based on topographic, demographic and histopathologic data with fair performance while maintaining transparency of the prediction.

5.1. Demographic seizure risk factors

Basic demographic data on age and gender is available at the beginning of the diagnostic process and thus potentially useful in predicting seizure risk. The described age-dependent risk profile, with a peak between 30 and 50 years, is consistent with some previous reports (Liigant et al., 2001), while others described the risk as increasing with age (Pallud et al., 2014) or considered age to be irrelevant (Chang et al., 2008). Whether age is an independent risk factor is questionable, as the observed differences may be explained by age-dependent histopathologic and topographic distributions. For instance, histopathologic entities of childhood and adolescence (e.g. pilocytic astrocytoma, medulloblastoma, ependymoma) and their preferred infratentorial location were associated with a low risk of seizures. No gender difference in seizure risk was observed, which is consistent with previous reports (Chang et al., 2008; Wilne et al., 2007).

5.2. Histopathologic seizure risk factors

Significant differences in seizure risk were observed between the histopathologic brain tumor entities and grades: Consistent with previous reports (Kerkhof and Vecht, 2013), a higher seizure risk in developmental tumors as well as low-grade tumors versus high-grade tumors was observed. Pilocytic astrocytoma, medulloblastoma and ependymoma showed low epileptogenic potential relative to glioblastoma. The lower seizure risk in metastases and PCNSL is consistent with previous literature (Lynam et al., 2007; van Breemen et al., 2007; Weller et al., 2012). These differences in seizure risk might be due to histopathologic tumor characteristics or due to the inherent topographic anatomical pattern of the various entities. Such patterns include: the preferably cortical location of developmental tumors; the involvement of the cerebral cortico-ventricular axis, typically of the insula or anterior temporal lobe, without diffuse invasion of the corpus callosum or subependymal ventricular wall in grade II and III gliomas; the infratentorial location of pilocytic astrocytoma, medulloblastoma and ependymoma; the common infratentorial location of metastases; or the diffuse invasion of the corpus callosum and the ventricular wall by PCNSL. The most plausible explanation seems to be that epileptogenicity is a combined effect of tumor-intrinsic molecular and histopathologic characteristics and the brain's anatomy (Akeret et al., 2019).

5.3. Topographic anatomical seizure risk factors

This study identified specific topographic anatomical brain tumor patterns to be associated with high or low seizure risk. The concept of pathoclisis implies a selective vulnerability of different areas of the brain to various diseases (Vogt and Vogt, 1922). Accordingly, anatomical regions differing in their histologic and molecular characteristics as well as their phylo- and ontogenetic background might exhibit different seizure risks.

The supratentorial lobar/gyral structures appear to be the most relevant ones regarding epileptogenicity. Whereas almost half of the patients with supratentorial tumors suffer from epileptic seizures, such are found in less than 1% of infratentorial tumors. Deep-seated supratentorial tumors (eg. basal ganglia, internal capsule, thalamus, septum pellucidum, choroid plexus) also have a much lower seizure risk.

Significant differences were also observed among the lobar and gyral structures, with the primary motor/somatosensory, mesopallial and allopallial structures found pro-epileptogenic. The central lobe (with the precentral gyrus, postcentral gyrus, subcentral gyrus and paracentral lobule) and the insular lobe (with the short and long insular gyri) showed the highest positive seizure risk difference. The posterior third of the superior and the middle frontal gyrus also had an increased seizure risk, both of which lie directly adjacent to the precentral gyrus. Similarly, the also adjoining pars opercularis of the inferior frontal gyrus showed the same tendency. An increased seizure risk was also found with the posterior orbital gyrus, rectal gyrus, the subcallosal area, temporal pole, the anterior third of the inferior temporal gyrus and the parahippocampal gyrus. This anatomical pro-epileptogenic pattern corresponds to the central and the mesopallial fronto-insulo-temporal structures. The allocortical hippocampus and amydala also showed an increased risk of seizures, as did the extreme and external capsule located below the insular cortex.

The cerebral structures associated with an increased seizure risk are characterized by a distinctive cortical microarchitecture and

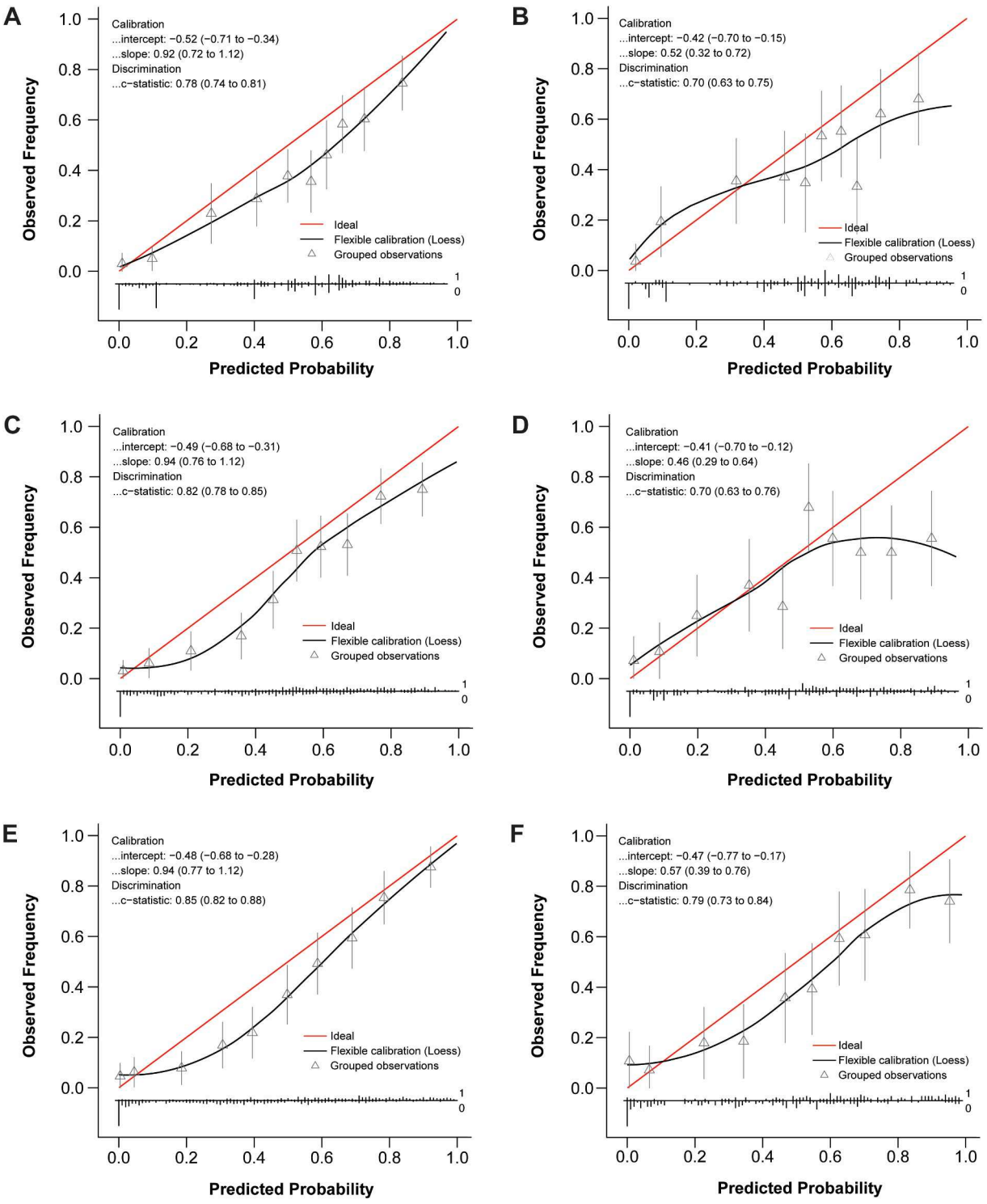

Fig. 4. Calibration curves of the three seizure risk prediction models Calibration curves of the *topographic* (T), *topographic/demographic* (TD) and *topographic/demographic/histopathologic* (TDH) models at bootstrap and internal validation after predictor selection by recursive feature elimination. The x axis demonstrates 10 bins of the probabilities predicted by the models, which are contrasted against the true observed frequency of the outcome on the y axis. A locally estimated scatterplot smoother (LOESS) curve is estimated over the 10 bins to arrive at a calibration curve. The red horizontal line demonstrates ideal calibration with an intercept of 0 and a slope of 1. Fig. 4A: Bootstrap of the *T model*. Fig. 4B: Internal validation of the *T model*. Fig. 4C: Bootstrap of the *TD model*. Fig. 4D: Internal validation of the *TD model*. Fig. 4E: Bootstrap of the *TDH model*. Fig. 4F: Internal validation of the *TDH model*. (For interpretation of the references to color in this figure legend, the reader is referred to the web version of this article.)

phylogenetic background, which might account for an increased structural epileptogenicity. The primary motor, supplementary motor and primary somatosensory cortices define the central lobe and adjacent areas (Brodmann areas 4, 6, 3, 1, 2) (Brodmann, 1909). Layer V of the primary motor cortex harbors the largest neurons of the body, the Betz' giant cells (Brodmann, 1909), which have been attested a particularly high epileptogenicity in electrophysiological studies (Chouinard and Paus, 2006; Telfeian and Connors, 1998). The posterior fronto-orbito-

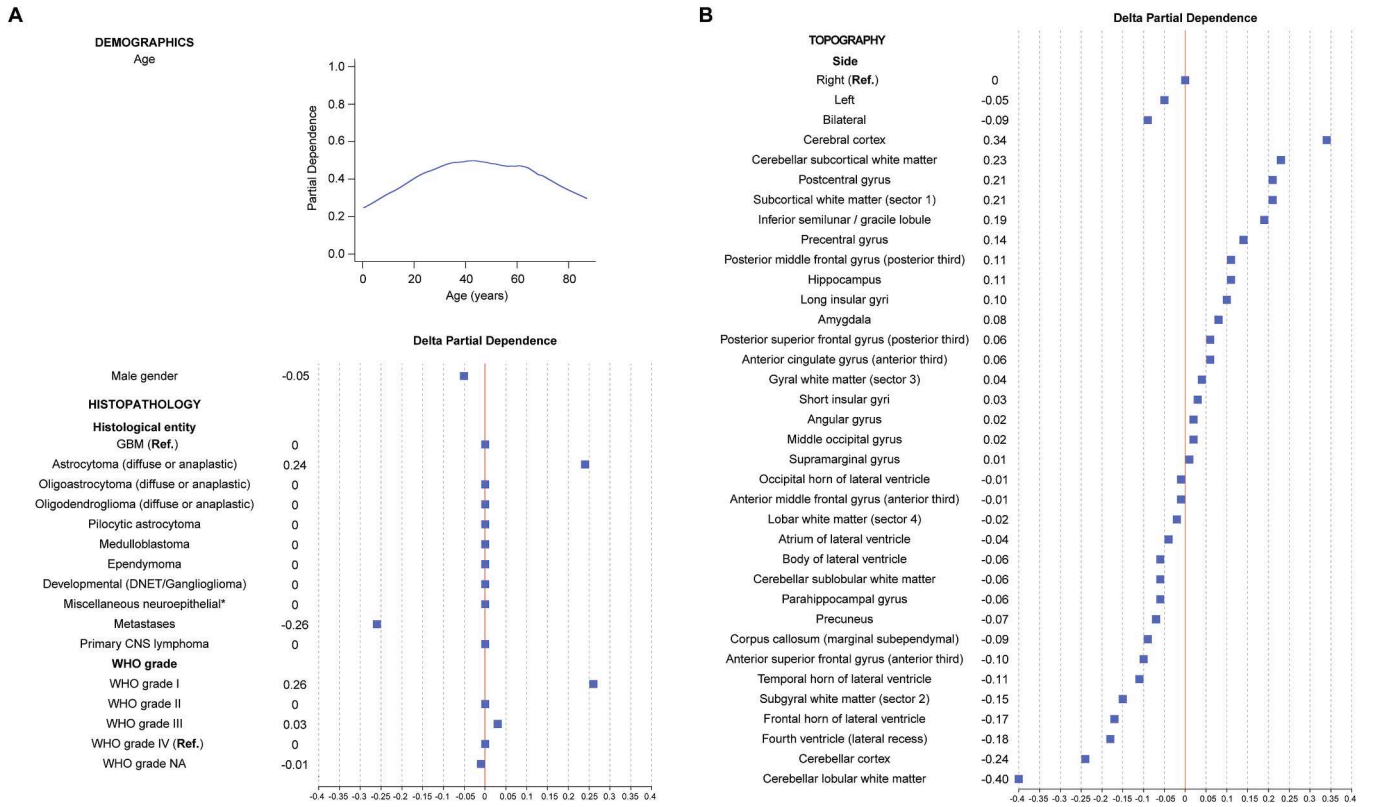

Fig. 5. Partial dependence in the TDH model Partial dependence on age and difference in partial dependence (delta partial dependence) of variables showing a differential marginal effect in the *topographic/demographic/ histopathologic* (TDH) model. Variables included in the model with partial dependence difference equal to 0 are not shown. Fig. 5A: Demographic and histopathologic (histologic entity and WHO grade) characteristics. Fig. 5B: Topographic anatomical characteristics.

mesial, the insular and the temporo-mesio-polar areas are mesocortical (Fleischhauer, 1976; Stephan, 1976; Vogt and Vogt, 1926; Zilles and Amunts, 2012). The amygdala and the hippocampus are allocortical (Fleischhauer, 1976; Stephan, 1976; Vogt and Vogt, 1926; Zilles and Amunts, 2012). Mesocortex and allocortex have a different cytoarchitecture than the neocortex and are phylogenetically older, which might be related to epileptogenicity. There is evidence based on animal models, electrophysiological studies, functional MRI studies and nuclear medicine studies that not only hippocampus and amygdala, but also the adjacent allo- and mesocortical areas have an increased potential for epileptogenicity (Avoli et al., 2002; Gale, 1988; Kelly and McIntyre, 1996; McIntyre and Gilby, 2008; Piredda and Gale, 1985; Uva et al., 2005; Vaughan and Jackson, 2014; Vismer et al., 2015). In particular, the piriform, perirhinal and entorhinal cortex have been identified as "trigger zones" for seizures. In experimental animal studies, these regions showed a particularly high sensitivity for the induction of seizures by chemical or electrical stimuli (Vaughan and Jackson, 2014; Vismer et al., 2015). While under physiological conditions there is rhythmic activity between these regions, malfunction seem to easily lead to pathological synchronization and spreading of epileptiform activity throughout the brain (Cataldi et al., 2013; McIntyre and Gilby, 2006; Vismer et al., 2015). The distinct cytoarchitecture as well as the pronounced local and long-range connections of these regions appear to be of pathophysiological relevance (Shepherd, 2011; Vaughan and Jackson, 2014; Vismer et al., 2015). In the rat, a pyramidal cell in the piriform cortex synapses with more than 1000 other cells, creating a large excitatory network (Johnson et al., 2000), requiring strong local feedback inhibition to prevent runaway activation (Franks et al., 2011). There are extensive connections between hippocampus, amygdala, piriform cortex, entorhinal cortex, orbitofronal cortex and agranular insular cortex (Burwell and Amaral, 1998; Johnson et al., 2000; Kajiwara et al., 2007; Krettek and Price, 1977; Shipley and Ennis, 1996). Numerous local recurrent circuits within this network can serve as substrates for seizure activity (Löscher and Ebert, 1996). The topographic anatomical brain tumor patterns identified in the current study, which appear to be associated with an increased seizure risk, all represent components of this phylogenetically older "olfactory network". The observation that the cingulate gyrus and the planum polare, which are also largely mesocortical, also tend to have a higher seizure risk, further supports this hypothesis. In contrast to this, adjacent neocortical structures (such as the planum temporale) show an opposite tendency. Even within the neocortex there are differences in seizure risks: a gradient is observed from the primary motor/somatosensory cortex to the frontal pole and the occipital pole, as well as from the temporal pole towards the occipital pole. This might also be phylogenetically determined by the differing character of the primary neocortical areas, the unimodal and the multimodal association cortices.

In addition to true differences in structural epileptogenicity, varying rates of seizure-detection might also contribute to the observed differences in seizure risk. Seizures originating in certain anatomical areas might have a more prominent clinical manifestation than others. Seizures with origin in the central lobe, for example, are expected to present with clinically apparent motor or somatosensory symptoms. Likewise, tumors of the mesopallial structures might indirectly impact on the central lobe through a space-occupying effect.

Deep-reaching lobar tumors appear to have a reduced seizure risk, which might be explained by the invasion and destruction of fiber tracts (i.e. short and long association fibers, commissural fibers), preventing the spread of epileptic activity that developed locally (most likely cortically). Within the gyral segments, the cortex showed the highest risk for seizures, decreasing progressively along the white matter sectors towards the ventricular wall. A reduced seizure risk was seen with involvement of the corpus callosum, but only in its central, i.e. fibrous part. The lower seizure risk seen with bilateral tumors might be

explainable by an expansion across the corpus callosum or a diencephalic/rhombencephalic tumor location.

5.4. Machine learning based prediction

In this study, we aimed to combine the elements of pathophysiological reasoning, transparent ML based modelling and clinical decision-making context. Machine learning provides new approaches for prediction, often outperforming conventional statistical methods (Rajkomar et al., 2019; Staartjes et al., 2018; Swinburne et al., 2019; Titano et al., 2018; van Niftrik et al., 2019). However, pathophysiological plausibility, transparency and clinical applicability remain important concerns, contributing to the limited translation into practice (Rajkomar et al., 2019). The scientific framework for the development of the model remains critical. Predictors must be available in the clinical decision situation, preferably display a pathophysiological plausibility, and the results of the prediction must impact clinical decision-making.

Both the performance and the transparency of the different models were taken into account in a preliminary analysis. Given the transparency provided by the PD analysis and comparable discrimination and calibration performance, GAMs were preferred to other algorithms.

To ensure clinical applicability, topographic, demographic and histopathologic input was implemented layer-wise in the model. All three models (*T*, *TD* and *TDH* GAM) showed a high performance. While the *TD* model failed to improve significantly over the *T* model, the *TDH* model demonstrated a further increase in performance.

Delta PD analysis allowed the model relevant input to be pathophysiologically reflected through comparison with the preceding inference analysis. The differentiation between dependence of a prediction model and causal interference should be an integral component of model development, understanding and translation. It has gained even more significance with ML based approaches, due to their often intransparent character. Delta PD of our *TDH* model was largely consistent with the results of the inference analysis. Some relevant differences, however, exist. The *TDH* model not only showed the expected dependence on age, but male gender was also a negative driver. This is likely explained by a higher incidence of metastases in males and not by a direct causal relationship. The dependence on histopathology only consists of metastases as negative driver and astrocytoma as well as WHO grade I as positive drivers. A plausible explanation is the unequal prevalence of the different tumor types with predominance of glioblastoma, metastases and astrocytoma (Akeret et al., 2020; Siegel et al., 2020). Certain cerebellar structures, such as the cerebellar subcortical white matter and the inferior semilunar/gracile lobules influence the prediction in the direction of “seizures”. However, assuming a causal relationship would be a wrong conclusion, as the inference analysis provided strong evidence against it. The fact that a subcortical cerebellar location in the inferior semilunar/gracile lobule is the most frequent manifestation of cerebellar metastases (Akeret et al., 2020) might be an explanation for the dependence of the model on these variables. The associated risk of concomitant supratentorial metastases and thus an increased risk of seizures might create this dependence.

6. Limitations and relevance

A practical limitation of the presented model is the inherent difficulty of localizing brain tumors in such detail, requiring profound anatomical knowledge and training. A simplified version will be required to establish a topographic anatomical model in clinical routine. The seizure risk driver identified in this study are a basis for such a simplified model. Another potential limitation consists in not including molecular tumor markers in the model. The relevance of such molecular markers in a seizure-risk prediction model applied at the time of initial diagnosis is limited due to the latency of the availability of such markers. Although this also applies to the histopathologic tumor entity, the latter can often be estimated or at least significantly limited by an experienced clinician based on the radiological appearance of the tumor. For this reason, gross histopathologic tumor entity was included in the TDH variant of our model, while molecular markers were not used. Clinical parameters were also excluded, as they show a high interrater variability and their pathophysiological relevance is questionable. Another clinical limitation is that seizures, especially non-motor seizures, are often underdiagnosed. Up to 50% of electrographic seizures remain unnoticed by the patient (Elger and Hoppe, 2018). In our center we attempt to keep this rate low by performing a long-term EEG in cases of unclear medical history to exclude tumor-related seizures. However, the possibility remains that in our cohort seizures, especially non-motor seizures, are underdiagnosed and that the correlations are influenced by a higher number of motor seizures compared to unrecognized non-motor seizures. A disadvantage of the selected study design with consecutive inclusion of all patients with first diagnosis of a primary or secondary brain tumor with any encephalic location is the resulting heterogeneity of the study population with limited statistical power for groups that are underrepresented (e.g. rare tumor entities). The advantage of this design, however, consists in its conformity to the clinical routine and therefore in its high generalizability. The design was aimed at simulating the clinical situation. A statistical limitation of this study is the high number of demographic, histopathologic and topographic parameters assessed and the associated problem of multiple hypothesis testing. This is an inherent limitation of the attempt of this study to consider all of the above variables collectively in terms of their interaction and pathophysiological plausibility. This limitation has been countered by using confidence intervals in the univariate analysis of seizure risk difference instead of p values to provide estimates of the magnitude and precision of the effect and to establish a pathophysiological plausibility evaluation rather than a mere quantification of the level of evidence for a difference. Some of the tested variables may be associated with each other, which might lead to less accurate estimates of the influence of individual variables and higher standard errors of the predictive performance measures through collinearity. A further limitation of this study is the relatively large ratio of tested predictors to patient numbers, which may limit the predictive performance of the final model by overfitting. These limitations were accepted, since it was not the aim of this study to develop a final predictive model, but rather to improve our pathophysiological understanding of brain tumor associated seizures and provide a basis for the development of a transparent prediction model. To establish a seizure risk prediction model for brain tumor patients, a simplification and a prospective, consecutive development study are required, followed by an impact study. The advantages of ML based methods should be used within this framework, but critically assessed for their pathophysiological plausibility.

7. Clinical implications

There are several potential clinical implications of a seizure risk prediction model. Even though prophylactic anti-epileptic therapy is not recommended by the ILAE and the American Association of Neurology (Glantz et al., 2000; Sirven et al., 2004; Tremont-Lukats et al., 2008) this issue remains controversial and the practice varies widely across different centers and countries. A survey conducted among neurosurgeons of the American Association of Neurological Surgeon revealed that, despite these guidelines, prophylactic antiepileptic therapy is installed in more than 70% of brain tumors at first diagnosis (Siomin et al., 2005). A stratification of these patients into seizure high-risk and low-risk at the time of diagnosis would considerably simplify the question of the risk-benefit ratio of prophylactic antiepileptic therapy and thus would have the potential to homogenize clinical practice. In addition to antiepileptic therapy, patient monitoring could also be adapted according to this risk stratification. Furthermore, this information could be incorporated into patient counselling regarding the potential antiepileptic effect of lifestyle changes (Rossetti and Stupp, 2010).

8. Conclusions

The present study highlights the relevance of the topographic anatomical tumor characteristics with respect to epileptogenicity and identifies specific phylogenetic anatomical patterns as epileptic drivers. Using a generalized additive model, the seizure risk can be predicted based on topographic, demographic and histopathologic data with fair performance while maintaining transparency of the prediction.

Declarations

We confirm that we have read the Journal's position on issues involved in ethical publication and affirm that this report is consistent with those guidelines.

Funding: Kevin Akeret is supported by the Prof. Dr. med. Karl und Rena Theiler-Haag foundation. Flavio Vasella is supported by the Emily Dorothy Lagemann (EMDO) foundation. Niklaus Krayenbühl is supported by the Swiss National Science Foundation (SNF).

Conflicts of interest/Competing interests: None of the authors has any conflict of interest to disclose.

Ethical approval: All procedures performed in studies involving human participants were in accordance with the ethical standards of the national research committee (Cantonal Ethics Committee Zürich, KEK 01120) and with the 1964 Helsinki declaration and its later amendments.

Consent to participate/Consent for publication: All patients or their legal representatives gave their written informed consent for participation and publication.

Availability of data and material: Additional data is made available in the supplementary methods and supplementary results online.

Code availability: The statistical software (R) code used is made available in the supplementary methods online.

Acknowledgments

We kindly thank Mr. Peter Roth for the artistic illustrations. This study was supported by the Prof. Dr. med. Karl und Rena Theiler-Haag foundation (grant No. 86101-26-01 to KA).

Appendix A. Supplementary data

Supplementary data to this article can be found online at https://doi.org/10.1016/j.nicl.2020.102506.

References

Abbasi, B., Goldenholz, D.M., 2019. Machine learning applications in epilepsy. Epilepsia. https://doi.org/10.1111/epi.16333.

Akeret, K., Serra, C., Rafi, O., Staartjes, V.E., Fierstra, J., Bellut, D., Maldaner, N., Imbach, L.L., Wolpert, F., Poryazova, R., Regli, L., Krayenbühl, N., 2019. Anatomical features of primary brain tumors affect seizure risk and semiology. NeuroImage. Clin. 22, 101688 https://doi.org/10.1016/j.nicl.2019.101688.

Akeret, K., Staartjes, V.E., Vasella, F., Serra, C., Fierstra, J., Neidert, M.C., Regli, L., Krayenbühl, N., 2020. Distinct topographic-anatomical patterns in primary and secondary brain tumors and their therapeutic potential. J. Neurooncol. https://doi.org/10.1007/s11060-020-03574-w.

Allen, W.E., 2009. Terminologia anatomica: international anatomical terminology and Terminologia Histologica: International Terms for Human Cytology and Histology. J. Anat. 215, 221–221. DOI:10.1111/j.1469-7580.2009.1093_1.x.

Arle, J.E., Perrine, K., Devinsky, O., Doyle, W.K., 1999. Neural network analysis of preoperative variables and outcome in epilepsy surgery. J. Neurosurg. 90, 998–1004. https://doi.org/10.3171/jns.1999.90.6.0998.

Avoli, M., D'Antuono, M., Louvel, J., Köhling, R., Biagini, G., Pumain, R., D'Arcangelo, G., Tancredi, V., 2002. Network and pharmacological mechanisms leading to epileptiform synchronization in the limbic system in vitro. Prog. Neurobiol. DOI: 10.1016/S0301-0082(02)00077-1.

Brodmann, K., 1909. Vergleichende Lokalisationslehre der Grosshirnrinde in ihren Prinzipien dargestellt auf Grund des Zellenbaues. Barth, Leipzig, pp. 1–324.

Burwell, R.D., Amaral, D.G., 1998. Cortical afferents of the perirhinal, postrhinal, and entorhinal cortices of the rat. J. Comp. Neurol. https://doi.org/10.1002/(SICI)1096-9861(19980824)398:2<179::AID-CNE3>3.0.CO;2-Y.

Cataldi, M., Avoli, M., De Villers-Sidani, E., 2013. Resting state networks in temporal lobe epilepsy. Epilepsia. https://doi.org/10.1111/epi.12400.

Chang, E.F., Potts, M.B., Keles, G.E., Lamborn, K.R., Chang, S.M., Barbaro, N.M., Berger, M.S., 2008. Seizure characteristics and control following resection in 332 patients with low-grade gliomas. J. Neurosurg. 108, 227–235. https://doi.org/10.3171/JNS/2008/108/2/0227.

Chouinard, P.A., Paus, T., 2006. The primary motor and premotor areas of the human cerebral cortex. Neuroscientist 12, 143–152. https://doi.org/10.1177/1073858405284255.

Elger, C.E., Hoppe, C., 2018. Diagnostic challenges in epilepsy: seizure under-reporting and seizure detection. Lancet Neurol. https://doi.org/10.1016/S1474-4422(18)30038-3.

Ertürk Çetin, Ö., İşler, C., Uzan, M., Özkara, Ç., 2017. Epilepsy-related brain tumors. Seizure. https://doi.org/10.1016/j.seizure.2016.12.012.

Fisher, R.S., Acevedo, C., Arzimanoglou, A., Bogacz, A., Cross, J.H., Elger, C.E., Engel, J., Forsgren, L., French, J.A., Glynn, M., Hesdorffer, D.C., Lee, B.I., Mathern, G.W., Moshé, S.L., Perucca, E., Scheffer, I.E., Tomson, T., Watanabe, M., Wiebe, S., 2014. ILAE Official Report: a practical clinical definition of epilepsy. Epilepsia 55, 475–482. https://doi.org/10.1111/epi.12550.

Fisher, R.S., Cross, J.H., French, J.A., Higurashi, N., Hirsch, E., Jansen, F.E., Lagae, L., Moshé, S.L., Peltola, J., Roulet Perez, E., Scheffer, I.E., Zuberi, S.M., 2017. Operational classification of seizure types by the International League Against Epilepsy: Position Paper of the ILAE Commission for Classification and Terminology. Epilepsia 58, 522–530. https://doi.org/10.1111/epi.13670.

Fleischhauer, K., 1976. Handbuch der mikroskopischen Anatomie des Menschen, Bd. 4, Teil 9: Nervensystem, Allocortex — bearbeitet von H. Stephan. Electroencephalogr. Clin. Neurophysiol. DOI:10.1016/0013-4694(76)90115-2.

Franks, K.M., Russo, M.J., Sosulski, D.L., Mulligan, A.A., Siegelbaum, S.A., Axel, R., 2011. Recurrent circuitry dynamically shapes the activation of piriform cortex. Neuron. https://doi.org/10.1016/j.neuron.2011.08.020.

Gale, K., 1988. Progression and generalization of seizure discharge: anatomical and neurochemical substrates. Epilepsia. https://doi.org/10.1111/j.1528-1157.1988.tb05795.x.

Glantz, M.J., Cole, B.F., Forsyth, P.A., Recht, L.D., Wen, P.Y., Chamberlain, M.C., Grossman, S.A., Cairncross, J.G., 2000. Practice parameter: anticonvulsant prophylaxis in patients with newly diagnosed brain tumors: report of the Quality Standards Subcommittee of the American Academy of Neurology. Neurology 54, 1886–1893. https://doi.org/10.1212/WNL.54.10.1886.

Gleichgerrcht, E., Munsell, B., Bhatia, S., Vandergrift, W.A., Rorden, C., McDonald, C., Edwards, J., Kuzniecky, R., Bonilha, L., 2018. Deep learning applied to whole-brain connectome to determine seizure control after epilepsy surgery. Epilepsia 59, 1643–1654. https://doi.org/10.1111/epi.14528.

Guyon, I., Weston, J., Barnhill, S., Vapnik, V., 2002. Gene selection for cancer classification using support vector machines. Mach. Learn. 389–422 (2002) https://doi.org/10.1023/A:1012487302797.

Hastie, T., Tibshirani, R., 1986. Generalized additive models. Stat. Sci. 1, 297–310. https://doi.org/10.1214/ss/1177013604.

Johnson, D.M.G., Illig, K.R., Behan, M., Haberly, L.B., 2000. New features of connectivity in piriform cortex visualized by intracellular injection of pyramidal cells suggest that "primary" olfactory cortex functions like "association" cortex in other sensory systems. J. Neurosci. https://doi.org/10.1523/jneurosci.20-18-06974.2000.

Kajiwara, R., Tominaga, T., Takashima, I., 2007. Olfactory information converges in the amygdaloid cortex via the piriform and entorhinal cortices: Observations in the guinea pig isolated whole-brain preparation. Eur. J. Neurosci. DOI:10.1111/j.1460-9568.2007.05610.x.

Kelly, M.E., McIntyre, D.C., 1996. Perirhinal cortex involvement in limbic kindled seizures, in: Epilepsy Research. DOI:10.1016/S0920-1211(96)00056-3.

Kerkhof, M., Vecht, C.J., 2013. Seizure characteristics and prognostic factors of gliomas. Epilepsia 54, 12–17. https://doi.org/10.1111/epi.12437.

Krettek, J.E., Price, J.L., 1977. Projections from the amygdaloid complex and adjacent olfactory structures to the entorhinal cortex and to the subiculum in the rat and cat. J. Comp. Neurol. https://doi.org/10.1002/cne.901720409.

Liigant, A., Haldre, S., Oun, A., Linnamägi, U., Saar, A., Asser, T., Kaasik, a E., 2001. Seizure disorders in patients with brain tumors. Eur. Neurol. 45, 46–51. https://doi.org/52089.

Löscher, W., Ebert, U., 1996. The role of the piriform cortex in kindling. Prog. Neurobiol. DOI:10.1016/S0301-0082(96)00036-6.

Lynam, L.M., Lyons, M.K., Drazkowski, J.F., Sirven, J.I., Noe, K.H., Zimmerman, R.S., Wilkens, J.A., 2007. Frequency of seizures in patients with newly diagnosed brain tumors: a retrospective review. Clin. Neurol. Neurosurg. 109, 634–638. https://doi.org/10.1016/j.clineuro.2007.05.017.

McIntyre, D.C., Gilby, K.L., 2008. Mapping seizure pathways in the temporal lobe, in: Epilepsia. DOI:10.1111/j.1528-1167.2008.01507.x.

McIntyre, D.C., Gilby, K.L., 2006. Parahippocampal networks, intractability, and the chronic epilepsy of kindling. Adv. Neurol.

Moons, K.G.M., Altman, D.G., Reitsma, J.B., Ioannidis, J.P.A., Macaskill, P., Steyerberg, E.W., Vickers, A.J., Ransohoff, D.F., Collins, G.S., 2015. Transparent Reporting of a multivariable prediction model for Individual Prognosis Or Diagnosis (TRIPOD): explanation and elaboration. Ann. Intern. Med. 162, W1. https://doi.org/10.7326/M14-0698.

Munsell, B.C., Wee, C.-Y., Keller, S.S., Weber, B., Elger, C., da Silva, L.A.T., Nesland, T., Styner, M., Shen, D., Bonilha, L., 2015. Evaluation of machine learning algorithms for treatment outcome prediction in patients with epilepsy based on structural connectome data. Neuroimage 118, 219–230. https://doi.org/10.1016/j.neuroimage.2015.06.008.

Pallud, J., Audureau, E., Blonski, M., Sanai, N., Bauchet, L., Fontaine, D., Mandonnet, E., Dezamis, E., Psimaras, D., Guyotat, J., Peruzzi, P., Page, P., Gal, B., Párraga, E., Baron, M.H., Vlaicu, M., Guillevin, R., De'aux, B., Duffau, H., Taillandier, L., Capelle,

L., Huberfeld, G., 2014. Epileptic seizures in diffuse low-grade gliomas in adults. Brain 137, 449–462. DOI:10.1093/brain/awt345.
Piredda, S., Gale, K., 1985. A crucial epileptogenic site in the deep prepiriform cortex. Nature. https://doi.org/10.1038/317623a0.
R Core Team, 2020. R: A Language and Environment for Statistical Computing.
Rajkomar, A., Dean, J., Kohane, I., 2019. Machine learning in medicine. N. Engl. J. Med. 380, 1347–1358. https://doi.org/10.1056/NEJMra1814259.
Rossetti, A.O., Stupp, R., 2010. Epilepsy in brain tumor patients. Curr. Opin. Neurol. DOI: 10.1097/WCO.0b013e32833e996c.
Sanson, M., Marie, Y., Paris, S., Idbaih, A., Laffaire, J., Ducray, F., Hallani, S. El, Boisselier, B., Mokhtari, K., Hoang-Xuan, K., Delattre, J.Y., 2009. Isocitrate dehydrogenase 1 codon 132 mutation is an important prognostic biomarker in gliomas. J. Clin. Oncol. 27, 4150–4154. https://doi.org/10.1200/JCO.2009.21.9832.
Shepherd, G.M., 2011. The microcircuit concept applied to cortical evolution: from three-layer to six-layer cortex. Front. Neuroanat. 5 https://doi.org/10.3389/fnana.2011.00030.
Shipley, M.T., Ennis, M., 1996. Functional organization of olfactory system. J. Neurobiol. https://doi.org/10.1002/(SICI)1097-4695(199605)30:1<123::AID-NEU11>3.0.CO;2-N.
Siegel, R.L., Miller, K.D., Jemal, A., 2020. Cancer statistics, 2020. CA. Cancer J. Clin. DOI:10.3322/caac.21590.
Siomin, V., Angelov, L., Li, L., Vogelbaum, M.A., 2005. Results of a survey of neurosurgical practice patterns regarding the prophylactic use of anti-epilepsy drugs in patients with brain tumors. J. Neurooncol. DOI:10.1007/s11060-004-6912-4.
Sirven, J.I., Wingerchuk, D.M., Drazkowski, J.F., Lyons, M.K., Zimmerman, R.S., 2004. Seizure prophylaxis in patients with brain tumors: a meta-analysis. Mayo Clin. Proc. 79, 1489–1494. https://doi.org/10.4065/79.12.1489.
Skardelly, M., Brendle, E., Noell, S., Behling, F., Wuttke, T.V., Schittenhelm, J., Bisdas, S., Meisner, C., Rona, S., Tatagiba, M.S., Tabatabai, G., 2015. Predictors of preoperative and early postoperative seizures in patients with intra-axial primary and metastatic brain tumors: a retrospective observational single center study. Ann. Neurol. 78, 917–928. https://doi.org/10.1002/ana.24522.
Staartjes, V.E., Schröder, M.L., 2018. Letter to the Editor. Class imbalance in machine learning for neurosurgical outcome prediction: are our models valid? J. Neurosurg. Spine 29, 611–612. https://doi.org/10.3171/2018.5.SPINE18543.
Staartjes, V.E., Serra, C., Muscas, G., Maldaner, N., Akeret, K., van Niftrik, C.H.B., Fierstra, J., Holzmann, D., Regli, L., 2018. Utility of deep neural networks in predicting gross-total resection after transsphenoidal surgery for pituitary adenoma: a pilot study. Neurosurg. Focus 45, E12. https://doi.org/10.3171/2018.8.FOCUS18243.
Stephan, H., 1976. Vergleichende Anatomie des Allocortex. Verh. Anat. Ges.
Swinburne, N.C., Schefflein, J., Sakai, Y., Oermann, E.K., Titano, J.J., Chen, I., Tadayon, S., Aggarwal, A., Doshi, A., Nael, K., 2019. Machine learning for semi-automated classification of glioblastoma, brain metastasis and central nervous system lymphoma using magnetic resonance advanced imaging. Ann. Transl. Med. 7, 232–232. DOI:10.21037/atm.2018.08.05.
Telfeian, A.E., Connors, B.W., 1998. Layer-specific pathways for the horizontal propagation of epileptiform discharges in neocortex. Epilepsia 39, 700–708. https://doi.org/10.1111/j.1528-1157.1998.tb01154.x.
Titano, J.J., Badgeley, M., Schefflein, J., Pain, M., Su, A., Cai, M., Swinburne, N., Zech, J., Kim, J., Bederson, J., Mocco, J., Drayer, B., Lehar, J., Cho, S., Costa, A., Oermann, E. K., 2018. Automated deep-neural-network surveillance of cranial images for acute neurologic events. Nat. Med. 24, 1337–1341. https://doi.org/10.1038/s41591-018-0147-y.
Tremont-Lukats, I.W., Ratilal, B.O., Armstrong, T., Gilbert, M.R., 2008. Antiepileptic drugs for preventing seizures in people with brain tumors. Cochrane database Syst. Rev. CD004424. DOI:10.1002/14651858.CD004424.pub2.
Uva, L., Librizzi, L., Wendling, F., De Curtis, M., 2005. Propagation dynamics of epileptiform activity acutely induced by bicuculline in the hippocampal-parahippocampal region of the isolated guinea pig brain. Epilepsia. https://doi.org/10.1111/j.1528-1167.2005.00342.x.
van Breemen, M.S.M., Wilms, E.B., Vecht, C.J., 2007. Epilepsy in patients with brain tumours: epidemiology, mechanisms, and management. Lancet Neurol. 6, 421–430. https://doi.org/10.1016/S1474-4422(07)70103-5.
van Niftrik, C.H.B., van der Wouden, F., Staartjes, V.E., Fierstra, J., Stienen, M.N., Akeret, K., Sebök, M., Fedele, T., Sarnthein, J., Bozinov, O., Krayenbühl, N., Regli, L., Serra, C., 2019. Machine learning algorithm identifies patients at high risk for early complications after intracranial tumor surgery: registry-based cohort study. Neurosurgery 85, E756–E764. https://doi.org/10.1093/neuros/nyz145.
Vaughan, D.N., Jackson, G.D., 2014. The piriform cortex and human focal epilepsy. Front. Neurol. DOI:10.3389/fneur.2014.00259.
Vismer, M.S., Forcelli, P.A., Skopin, M.D., Gale, K., Koubeissi, M.Z., 2015. The piriform, perirhinal, and entorhinal cortex in seizure generation. Front. Neural Circuits 9. https://doi.org/10.3389/fncir.2015.00027.
Vogt, C., Vogt, O., 1922. Erkrankungen der Grosshirnrinde im Lichte der Topistik, Pathoklise und Pathoarchitektonik. J. Psychiatr. Neurol. 28, 1–73.
Vogt, C., Vogt, O., 1926. Die vergleichend-architektonische und die vergleichend-reizphysiologische Felderung der Grosshirnrinde unter besonderer Berücksichtigung der menschlichen. Naturwissenschaften 14, 1190–1194. https://doi.org/10.1007/BF01451766.
von Elm, E., Altman, D.G., Egger, M., Pocock, S.J., Gøtzsche, P.C., Vandenbroucke, J.P., 2007. The Strengthening the Reporting of Observational Studies in Epidemiology (STROBE) statement: guidelines for reporting observational studies. Lancet 370, 1453–1457. https://doi.org/10.1016/S0140-6736(07)61602-X.
Weller, M., Stupp, R., Wick, W., 2012. Epilepsy meets cancer: when, why, and what to do about it? Lancet Oncol. 13, e375–e382. https://doi.org/10.1016/S1470-2045(12)70266-8.
Wilne, S., Collier, J., Kennedy, C., Koller, K., Grundy, R., Walker, D., 2007. Presentation of childhood CNS tumours: a systematic review and meta-analysis. Lancet Oncol. 8, 685–695. https://doi.org/10.1016/S1470-2045(07)70207-3.
Zilles, K., Amunts, K., 2012. Architecture of the cerebral cortex. In: The Human Nervous System. Elsevier, pp. 836–895. https://doi.org/10.1016/B978-0-12-374236-0.10023-9.